applied sciences

MDPI

Review

Noble Metal-Based Heterogeneous Catalysts for Electrochemical Hydrogen Evolution Reaction

Huajie Niu, Qingyan Wang, Chuanxue Huang, Mengyang Zhang, Yu Yan, Tong Liu and Wei Zhou *

School of Chemistry, Beijing Advanced Innovation Center for Biomedical Engineering, Beihang University, Beijing 100191, China
* Correspondence: zhouwei@buaa.edu.cn

Abstract: Hydrogen energy, a green renewable energy, has shown great potential in developing new energy and alleviating environmental problems. Water electrolysis is an effective method to achieve large-scale clean hydrogen production, but this process needs to consume a huge amount of electric energy. It is urgent to develop high-activity, high-stability and low-cost catalysts to reduce the consumption of electric energy. At present, the noble metal catalyst is the star material in the hydrogen evolution reaction (HER), but its stability and high cost restrict its large-scale application. In this review, we comprehensively discussed the research progress on noble metal-based heterogeneous electrocatalysts used in water electrolysis for hydrogen production. Firstly, we analyzed the influence factors for hydrogen production performance, including the mass transfer process, the adsorption–desorption process, the catalytic process, and the influence of the working electrode and electrolyte. Then, we discussed the relationship between catalytic activity and electronic structure and chemical composition in view of theoretical calculations and summarized the strategies for developing efficient catalysts (alloying and interface engineering). Finally, we highlighted the challenges for the practical application of noble metal-based hydrogen evolution electrocatalysts.

Keywords: precious metal; heterogeneous catalyst; hydrogen evolution reaction; alloying; interface engineering

check for updates

Citation: Niu, H.; Wang, Q.; Huang, C.; Zhang, M.; Yan, Y.; Liu, T.; Zhou, W. Noble Metal-Based Heterogeneous Catalysts for Electrochemical Hydrogen Evolution Reaction. *Appl. Sci.* **2023**, *13*, 2177. https://doi.org/10.3390/app13042177

Received: 31 December 2022
Revised: 1 February 2023
Accepted: 3 February 2023
Published: 8 February 2023

Copyright: © 2023 by the authors. Licensee MDPI, Basel, Switzerland. This article is an open access article distributed under the terms and conditions of the Creative Commons Attribution (CC BY) license (https://creativecommons.org/licenses/by/4.0/).

1. Introduction

The massive use of coal, oil and natural gas not only causes the depletion of traditional fossil energy worldwide but also brings serious environmental problems such as the greenhouse effect. Hydrogen energy, a clean, sustainable new energy with high calorific value, can replace traditional fossil fuels, which has great potential for solving the global energy shortage and environmental problems [1,2]. The steam reforming process is commonly used to produce hydrogen in industry. However, this process needs high reaction temperatures, generates a large amount of carbon dioxide, and produces hydrogen with sulfur-containing impurities that have a great impact on the environment and are easy to poison catalysts [3,4]. Water electrolysis has attracted the wide attention of researchers for hydrogen production. Because this process requires only electricity and water, and the raw materials are plentiful and cheap. In addition, the conversion rate of water splitting to produce hydrogen and oxygen is as high as 80% from the perspective of thermodynamics [5]. However, the bottleneck factor in the water electrolysis hydrogen production is the need to provide additional electrical energy to overcome the energy barrier in water electrolysis—overpotential (η, i.e., the difference between the actual voltage values of the electrochemical reaction and the theory of thermodynamics, including the interface potential difference between the electrode and the electrolyte solution, and the contact potential between the two electrodes and electric and conductor). Given the current sources of electricity, developing new forms of electricity is also another way to reduce the cost of producing hydrogen. Based on the abundant solar, wind and ocean energy in

nature, the cost of hydrogen production will be greatly reduced by combining photovoltaic and wind power generation and triboelectric nanogenerator (TENG) using ocean energy with water electrolytic equipment [6,7]. Therefore, it is necessary to develop high-efficient electrocatalysts and new electricity sources to overcome the overpotential and improve the energy conversion efficiency of electric energy to chemical energy.

At present, noble metal-based materials are the most efficient catalysts for the HER (Hydrogen Evolution Reaction), because their ΔG_{H^*} is close to zero, which is the most optimized hydrogen adsorption free energy [8]. However, their practicability is greatly reduced due to the high price and insufficient reserves of precious metals, as well as the dissolution, agglomeration and poisoning in the electrocatalytic process [9]. One of the major challenges of noble metal catalysis is to improve the utilization efficiency, stability and durability of the noble metal atoms without reducing catalyst activity. Therefore, researchers adopted a variety of strategies to design and synthesize noble metal-based catalysts, such as heteroatom doping, alloying, interface engineering, and introducing defects. In addition, many factors including the particle size, shape and metal–support interfaces can have significant influences on the catalytic properties of noble metal catalysts [10]. Meanwhile, some noble metal catalysts with different morphology and structures, such as a variety of hollow structures [11] and even single atom catalysts [12,13], were designed to achieve the goal of hydrogen economy using efficient hydrogen production. In addition, optimizing the electrode preparation method and selecting the appropriate electrolyte can also maximize the use of the catalyst during the electrolytic process, further improving the efficiency of hydrogen production [14–16].

In this review, we first summarize several factors affecting the HER electrocatalytic performance, including the mass transfer process, adsorption–desorption process, catalytic process and the influence of electrodes and electrolytes. Then, we introduce the catalytic mechanism of catalyst promoting hydrogen evolution. The research progress of noble metal-based materials in the electrocatalytic HER field is also summarized, mainly focusing on the structure of catalysts, including alloying and interface engineering. Finally, we highlight the challenges and application prospects of developing sustainable clean hydrogen-energy catalysts based on noble metals.

2. Factors That Affect HER Performance

The HER is a multiphase process that occurs on the surface of a solid electrocatalyst, including four consecutive steps of mass transmission, adsorption, reaction and desorption (Figure 1). It is necessary to fully consider the influence of the catalyst, working electrode and electrolyte on the above steps to improve the HER performance comprehensively.

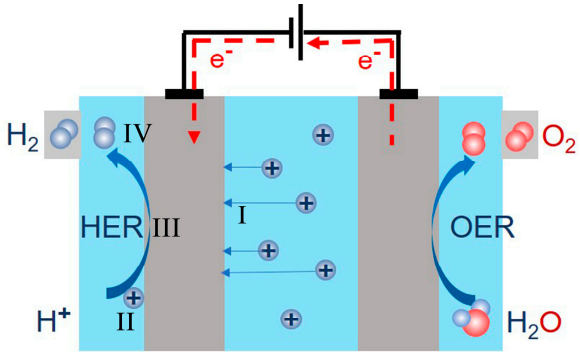

I mass transfer (H_3O^+(electrolyte) →H_3O^+(surface of the electrode))
II H_3O^+ absorption
III $2H_3O^+ + 2e^- \rightarrow H_2 + 2H_2O$
IV H_2 desorption

Figure 1. Schematic of a two–electrode water electrolyzer in an acidic electrolyte.

2.1. Mass Transfer Process

Many research works have shown that the mass transfer of nanocatalysis is very important to the whole catalytic process. Favorable mass transfer can improve the HER kinetics to a large extent [17,18]. For example, the mass transfer of the HER in an acidic electrolyte is H_3O^+ (solution body) $\rightarrow$ H_3O^+ (liquid layer near the electrode surface). The influence of ion migration can be minimized by increasing agitation, increasing the concentration of hydrogen ions in the electrolyte and changing the distance between the two electrodes [19]. As for the electrode, the surface structure of the electrode attached to the catalytic material and its loading amount (thickness) also have an important influence on mass transfer.

Some unique structures of catalysts have been shown to play a crucial role in mass transfer, such as ordered porous structures [20–22]. Sun et al. [23] prepared a three-dimensional ordered macroporous/mesoporous nickel using the wet chemical method. Combining ordered bi-continuous mesoporous and three-dimensional connected periodic microporous structures can realize highly efficient mass transfer. Ge et al. [21] prepared an ultrathin palladium network (Pd NMs) with a thickness of about 3 nm using solution oxidation etching, whose unique ordered mesoporous structure could realize rapid mass transfer. This catalyst embedded Pt nanoparticles into Pd NMs, and the resulting Pd NMs/Pt had extremely high HER activity and durability in acidic conditions. In addition, noble metal catalysts can be combined with other porous structures [24]. The porous shell structure facilitates the reactant to reach the active center on the inner surface of the shell through diffusion and mass transport [24]. However, the constructed porous structure is often hard to accurately regulate and appears disorderly, resulting in insufficient pore utilization. Irregular pore arrangement and/or tortuous pore channels are not conducive to rapid mass transfer in catalytic reactions [22]. Therefore, ordered porous structures are more advantageous for energy storage and conversion due to their efficient mass transfer.

In terms of basic research, the influence of the catalytic material loaded on the working electrode in mass transmission should not be ignored [14]. If the loading amount is too low, the coating slurry cannot completely cover the electrode surface and there will not be enough catalytic active sites. If the loading amount is too high, the aggregation of catalytic materials will affect the contact between the active components and the electrolyte, further influencing the mass transfer process. The thickness of the coating paste is usually controlled to be a few microns thick, and the thickness can be determined with cross-section measurements [25] using a scanning electron microscope (SEM) or numerical estimation. In addition, too much Nafion (binder) in the coating slurry will form a thicker Nafion film, resulting in additional mass transfer resistance within the Nafion layer [26]. Therefore, to ensure that the diffusion resistance of the Nafion film is negligible, it is very important to optimize the additive amount of Nafion [26].

2.2. Adsorption and Desorption Process

Due to the low conductivity of pure water, adding a strong acid, strong base or salt into the water can form a high-conductivity electrolyte for the HER process. Therefore, different electrolyte states (different pH values) produce different catalytic mechanisms of adsorption and desorption.

Under acidic conditions, H^+ or H_3O^+ is adsorbed at the active site after the mass transfer process, that is, the Volmer reaction, as shown in Equation (1) (* represents adsorption site):

$$H_3O^+ + e^- \rightarrow H^* + H_2O \quad (1)$$

There are two possible desorption steps, which are the electrochemical desorption step, namely the Heyrovsky reaction, as shown in Equation (2), or the chemical desorption step, namely the Tafel reaction, as shown in Equation (3):

$$H^* + H_3O+ + e^- \rightarrow H_2 + H_2O \quad (2)$$

$$H^* + H^* \rightarrow H_2 \quad (3)$$

Under alkaline conditions, the electrochemical adsorption step (the Volmer reaction) occurs first, as shown in Equation (4):

$$H_2O + e^- \rightarrow H^* + OH^- \quad (4)$$

There are also two possible desorption steps, namely electrochemical desorption (the Heyrovsky reaction), as shown in Equation (5), or chemical desorption (the Tafel reaction), as shown in Equation (3):

$$H^* + H_2O + e^- \rightarrow H_2 + OH^- \quad (5)$$

The rate of adsorption and desorption affects the overall HER kinetics. Generally, Tafel slopes of 120, 40 and 30 mV dec^{-1} were observed for the Volmer, Heyrovsky and Tafel determining rate steps, respectively. Additionally, for the Volmer rate-determining step, a Tafel slope of 120 mV dec^{-1} was observed in the higher coverage region ($\theta_H > 0.6$). Therefore, the rate-determining step of the HER can be judged from the Tafel slope. Tafel formula is shown in Equation (6):

$$\eta = b \log |j| + a \quad (6)$$

where η is the hydrogen evolution overpotential, j is the current density, b is the Tafel slope and a is the overpotential value when the current density is 1 A cm^{-2}. According to the value of a, the metals can be divided into the following three categories: high overpotential metals (a $\approx$ 1.0~1.5 V), mainly including Pb, Cd, Hg, Tl, Zn, Ga, Bi, Sn, etc.; medium overpotential metals (a $\approx$ 0.5~0.7 V), mostly including Fe, Co, Ni, Cu, W, Au, etc.; low overpotential metals (a $\approx$ 0.1~0.3 V), usually including some platinum group metals such as Pt, Pd and Ru [27]. The Tafel slope can be obtained with the linear part of the Tafel curve. If the Tafel slope value is about 120 mV dec^{-1}, the Volmer reaction is the rate-determining step. If the Tafel slope value is about 40 mV dec^{-1}, the electrochemical desorption process is the rate-determining step, corresponding to the Heyrovsky reaction. If the Tafel slope value is about 30 mV dec^{-1}, the rate-determining step is a chemical desorption reaction, corresponding to the Tafel reaction [28]. A smaller value of b means a smaller requirement of η to achieve the same current density and a faster transfer kinetic of the electrons. The surface electronic structure of the catalyst is a key factor affecting the adsorption and desorption of hydrogen. Therefore, designing an excellent HER catalyst by modulating the surface electronic structure is important to improve the overall kinetics of the HER.

2.3. Catalytic Process

In the catalytic process, it is essential that the catalyst provides the active surface. The reaction molecules adsorb on the surface, further form transition intermediates, and finally improve the reaction efficiency. Therefore, the bonding ability of the catalyst surface (i.e., the surface reactivity) can be used to describe the catalytic ability of the catalyst [29]. The HER is an electron-receiving reaction in which the electrons provided by the external electric field are transported to the reaction molecule through the conductive electrode, and then the electrochemical reaction occurs. In the case of the precious metal HER catalyst on the electrode surface, the adsorption of the metal surface often involves electrons from the metal surface to adsorbate, so the surface activity of the metal usually means the ability to provide electrons to the absorbed molecule from the metal surface. The effect of catalysts on the HER activity includes three aspects: the electronic structure effect, the surface structure effect and the geometric structure. In fact, there is a link among these aspects, and they affect each other. The electronic structure effect mainly refers to the influence on the activation energy from the energy band and surface state density. The surface structure effect refers to the catalyst regulating the number of active sites on the surface through the surface structure (such as atomic arrangement structure) to affect the reaction rate. The geometric structure refers to the morphology of the catalyst, which can also

affect the surface structure. When selecting the appropriate electrocatalyst, the electronic effect (composition matching) should be considered first to make the reaction activation energy appropriate (the change in activation energy can adjust the reaction rate by several to dozens of orders of magnitude). The catalytic performance can then be fine-tuned by modulating the surface structure effect or geometry structure [30].

2.3.1. Electron Structure Effect

The HER activity of precious metals Pt, Pd, Rh, and Ir is significantly better than other non-precious transition metal-based catalysts [9]. The differences in activity can be described by the d band energy center (ε_d), the vacant d orbital and the proportion of d electrons participating in the coordination. Figure 2 is a periodic table of transition metals containing valence electron configuration, ε_d and the proportion of d electrons [31]. In the table, the change in metal surface activity weakens from left to right in the same period, and this trend is related to ε_d. The ε_d gradually decreases from left to right in the periodic table, which means that the unfilled anti-bonding energy series of the d band decreases and the ability to adsorb electrons is enhanced. For transition metals in the same period, the energy compatibility with the front orbital of the adsorbed molecules is crucial. The d-block elements have empty d-orbitals, and the d-orbitals of the ds-block elements are fully filled with electrons. The catalytic activity is proportional to the proportion of d electrons involved in the coordination. As can be seen from Figure 2, for the d-block elements, the proportion of d electrons is above 0.6 for the VIII group metals, and the proportion of other transition metal elements is less than or equal to 0.6. However, the ε_d values of Fe, Co and Ni are larger than those of the platinum group elements, resulting in enhanced adsorption and decreased activity. In summary, from the perspective of electronic structure analysis, it can be concluded that the excellent catalytic performance of precious metals is due to low ε_d, vacant d orbitals that can participate in bonding and a high d electron ratio.

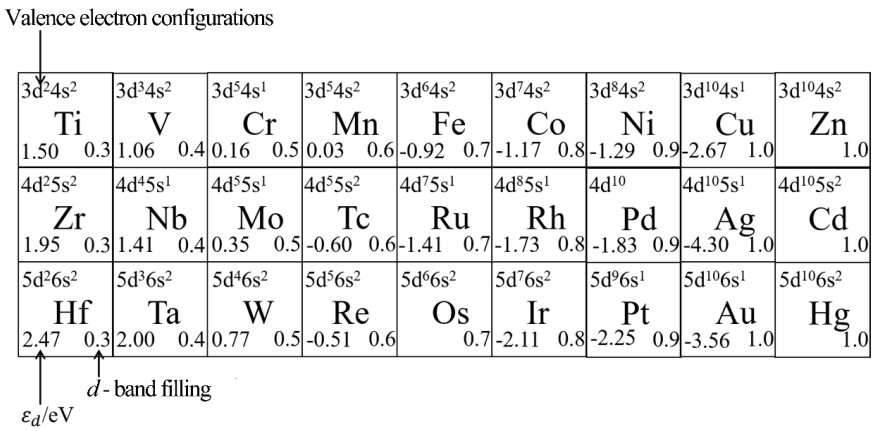

Figure 2. Periodic table of transition metals containing valence electron configurations, d and idealized d–band filling [31]. Copyright 2019, Royal Society of Chemistry.

2.3.2. Surface Structure Effect

Noble metal catalysts with the same composition and different exposed crystal surfaces have different catalytic performances. The research results show that the catalytic performance is closely related to the atomic arrangement and coordination number on the exposed surface. For precious metal crystals with the face-centered cubic (*fcc*) structure, the crystal surface can be divided into low-index crystal surfaces, including three fundamentals (111), (100) and (110), and high-index crystal surfaces (hkl)($h \geq k \geq l > 0$). In general, the nanocrystals with low-index surfaces have high coordination numbers and relatively low catalytic performance. Under normal conditions, the surface energy (γ) of the exposed surface follows $\gamma(111) < \gamma(100) < \gamma(110) < \gamma(hkl)$, such as Pt. The difference in surface reactivity caused by the atomic arrangement belongs to the electronic structure

effect. Compared with low-index surfaces, the precious metal polyhedrons with high-index surfaces contain multiple crystal orders, twin grain boundaries, crystal edges, vertexes and corners [32]. These structures have more abundant defects and low coordination active centers, which are easier to bind with the catalyzed substances and show excellent catalytic performance [33,34]. Therefore, developing noble metal nanostructures with high-index crystal surfaces is one of the effective ways to improve catalytic performance.

2.3.3. Geometric Structure Effect

In addition to the influence of the special crystal surfaces mentioned above, the dimension and density of the material (solid or hollow) also have an influence on the catalytic performance. For solid nanoparticles, only the surface atoms act as the active sites to catalyze. Especially for precious metals, in which the internal atoms cannot be utilized, this results in great waste. According to this, hollow structures such as nanoframes, nanocages, core–shell structures and porous structures can be constructed [35], which are lighter than solid particles and have a higher specific surface area and more efficient utilization of atoms. Therefore, atomic clusters and single-atom catalysts have attracted extensive attention. They have extremely high atomic economic benefits and unique geometric configurations and electronic structures [36,37], so their catalytic activity is significantly improved compared with the corresponding bulk-phase and solid nanoparticles. However, clusters and single atoms can easily aggregate due to their high surface energy. Therefore, substrates are often introduced to stabilize the clusters and single atoms, such as C, C–N and a metal–organic framework.

In essence, the fundamental characteristic that affects the catalytic activity is the outer electronic structure of the catalyst. It is the surface layer of the catalyst rather than the body that plays a crucial role in catalysis, so appropriate strategies should be adopted to modulate the surface electronic structure. Many studies have shown that alloying and interface engineering are effective strategies for regulating the surface electronic structure of catalysts, which will be described in detail in Section 4.

2.4. Influence of the Working Electrode

In order to characterize the intrinsic catalytic activity as close as possible to the catalytic material, the preparation of working electrodes is of great importance in basic laboratory research.

The working electrode refers to the electrode that can cause significant changes in the concentration of the components to be measured in the test solution during the test process, such as a glassy carbon electrode and platinum electrode. Generally, the bubbles generated on the electrode surface easily adhere to the surface of the catalyst, which makes the electrolyte mass transfer difficult. To solve this problem, Frumkin et al. first developed a high-speed rotating electrode, namely the RDE (Rotating Disk Electrode) [38]. Later, it was popularized by Schmidt et al. [39] using ink injection electrodes. Under high-speed rotation, the adverse effect of a large number of bubbles on the surface of the catalytic material is eliminated. The RDE is applicable to the three-electrode system. Figure 3a shows five electrolytic cells. The largest port in the middle is the working electrode and the rotating rod, while the other four ports are the counter electrode, the reference electrode, the air inlet (the required saturated gas should be passed into the electrolyte before the test) and the air outlet, and the placement position is not required [14]. The most common configuration of the RDE is a Teflon shell (length: 27 mm, diameter: 15 mm) wrapped with a glassy carbon electrode (diameter: 5 mm); the conductive flat glass carbon electrode on the RDE end face is used as a collector. The drip method is used to uniformly cover the glass carbon with the highly dispersed catalyst slurry prepared by the catalysts, binders and solvent. Some researchers also use carbon cloth, nickel foam and other rough substrate-supported catalysts with higher specific surfaces to improve stability. Although these are feasible paths, the substrate itself will have a better or worse effect on the catalytic performance [40].

The catalyst ink is generally composed of a catalyst with mass fraction w = 0.5–1.2%, deionized water with w = 0.6–1.1%, Nafion binder with w = 0.9–1.3% and solvent with w = 90–99% (including ethanol, isopropyl alcohol, n-propyl alcohol or n-butanol in any one or more combinations).

The conventional preparation process is as follows: the catalyst, deionized water, solvent and binder are added into glass bottles or centrifugal tubes and then mixed with ultrasonic for 30–60 min until it is uniform to obtain catalyst slurry. Considering the mass transfer problem, the amount of catalyst should be appropriate, and the amount of Nafion should be as little as possible [41]. In addition, the electrode preparation of some catalyst particles requires the addition of a conductive agent (without significant interference to the structure or properties of the catalyst). For the HER, high specific surface area carbon (such as TKK, Vulcan or Ketjen Black) is a good choice. Conductive additives can disperse catalyst particles to avoid agglomeration and ensure fast electron transport.

For the HER, the commercial Pt/C catalyst is often used for comparison samples, which is made with 46 wt% Pt loaded on high specific surface area carbon TKK (Tanaka Kikinzoku, Kogyo, Japan). The preparation was as follows: the glassy carbon electrode was polished with 0.05 μm alumina paste (initially large, then reduced to 0.05 μm) to achieve a mirror finish, cleaned repeatedly with ultrasonic waves in deionized water and dried for use under ambient conditions. The Pt/C and Nafion binders were dispersed in deionized water (18.2 MΩ cm, Millipore) and then treated with ultrasound in an ice bath for 30 min to obtain a homogeneous catalyst ink consisting of 0.15 $mg_{Pt/C}$ mL^{-1} and 0.04 mg_{Nafion} mL^{-1}. The RDE (diameter: 5 mm) was uniformly coated with 20 μL ink to obtain a platinum loading capacity of ~7.0 μg_{Pt} $cm^{-2}{}_{disk}$ [42]. The coating concentration and thickness can be adjusted according to specific experiments.

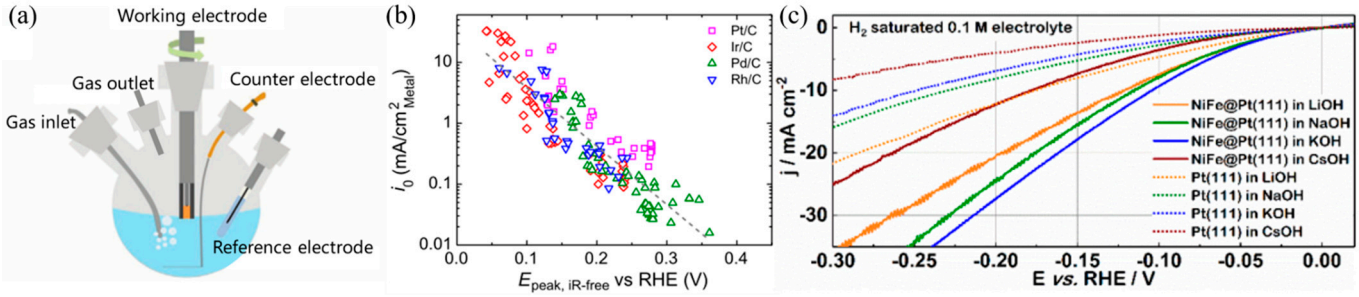

Figure 3. (**a**) Schematic of the electrolyzer for the rotating disk electrode (RDE) [14]; (**b**) Correlation between the exchange current density of the HOR/HER and H_{upd} desorption peak potential [15]; (**c**) The polarization curves of Pt (111) and NiFe@Pt (111) electrocatalysts (Ni:Fe ratio of 1:1) were recorded in different alkaline solutions recorded at a rotation rate of 1600 rpm and a scan rate of 50 mV s^{-1} [43]. Copyright 2019, 2020 John Wiley and Sons.

The traditional drip-coated electrode preparation process is an effective method to evaluate the activity of an electrocatalyst, but it will inevitably lead to uneven electrode interfaces. A large number of dead zones and high resistances are caused by the use of a binder, and even the catalyst will strip during gas production [44]. In order to obtain the best reaction conditions, we expect the working electrode to have a stable and good electrochemical interface. Researchers have developed self-supporting electrodes without binder, especially by directly depositing active materials on the substrate, which makes the overall catalytic efficiency and stability higher [45,46]. For example, Xiao et al. [16] used conductive nickel foam (NF) as a substrate to support an (Fe, Ni)$(OH)_2$ nanosheet array, which reduced Ru (III) to metal Ru and formed a three-dimensional self-supported Ru/(Fe, Ni)$(OH)_2$/NF with a super-hydrophilic surface and high conductivity. It ensured rapid gas release, efficient electron transport and mass transfer under high current density. It exhibited an overpotential of 152 mV to afford 1 A cm^{-2} in 1 M KOH, and it had good stability at high current density. In addition, electrodeposition is a very effective method to

immobilize electrocatalysts on the substrate for efficient water splitting. This method can prepare homogeneous films with abundant active centers in a few seconds [47]. Therefore, optimizing electrode preparation parameters is also an important link for more accurately detecting intrinsic activity and realizing the practical promotion of the catalyst.

2.5. Influence of the Electrolyte

The kinetics of Pt, Ir and Pd are two orders of magnitude slower in an alkaline medium (1 M KOH) than in an acidic medium (0.5 M H_2SO_4). Under the same overpotential, a higher load of precious metal is required on the negative electrode in an alkaline environment [48]. Therefore, the regulation of the HER catalytic activity can be achieved by optimizing the catalyst environment, namely by selecting the appropriate electrolyte.

Zheng et al. [15] studied the relationship between the HER catalyst activity and pH value of four supported platinum group metal catalysts (Pt/C, Ir/C, Pd/C and Rh/C) using cyclic voltammetry and the rotating disk electrode method in a wide pH range (0–13) (Figure 3b). The exchange current density (j_0) of the four catalysts decreased with the increase in pH. Their HER activity decreased with the increase in pH, while their slope was similar, indicating that the effect of pH on the HER activity was independent of the catalyst composition. In addition, the HER activity has a small change in different buffer solutions with similar pH values (phosphoric acid/phosphate, citric acid/citrate, acetic acid/acetate, carbonate/bicarbonate and boric acid/borate), suggesting that the properties of anions and adsorption had no significant effect on the HER activity.

Bandarenka and co-works [49,50] reported that the HER activity on the surface of platinum-based catalysts could be adjusted by changing the type of alkali metal cations in the electrolyte. Figure 3c shows the effect of metal cations (Li^+, Na^+, K^+, and Cs^+) on the HER activity in a 0.1 M H_2-saturated alkaline electrolyte using NiFe cluster-modified Pt (111) as the model catalyst. When KOH was used instead of CsOH, the HER activity of this electrode could be increased by nearly 3 times [43], confirming that cations regulating electrolytes contribute to the improvement of catalytic activity [51]. KOH solution is usually used to study the HER performance of catalysts under alkaline conditions because K^+ has better molar ionic conductivity than Na^+ (0.0735 vs. 0.0501 S L mol^{-1} cm^{-1}) [52].

3. Catalytic Mechanism of the HER

3.1. Volcano Plot

The "volcano plot", first established by Parsons, connects the value of j_0 with ΔG_{H^*} calculated using the Density Functional Theory (DFT) to describe the adsorption strength of H* on the catalyst surface [53]. Later, based on experiments, researchers established the "volcano plot" (Figure 4a) using the correlation between j_0 values of some elements and ΔG_{H^*} calculated using the DFT [8]. $\Delta G_{H^*} < 0$ indicates that the adsorption of H* is too strong and the desorption of H_2 is not sufficient, which causes the active centers on the catalyst to be blocked, thus resulting in catalyst poisoning and hindering the reaction from proceeding [54,55]. $\Delta G_{H^*} > 0$ means the adsorption of H* is too weak. The hydrogen atoms are not easily absorbed on the metal surface, and the coverage of hydrogen on the material surface is reduced, which causes the active center to not be effectively utilized, further slowing down the reaction speed [56]. Therefore, the energy of the intermediate is neither too strong nor too weak on the surface for an ideal catalyst. It can be seen from the figure that the platinum group precious metals located at the vertex of the volcanic curve have the best HER activity.

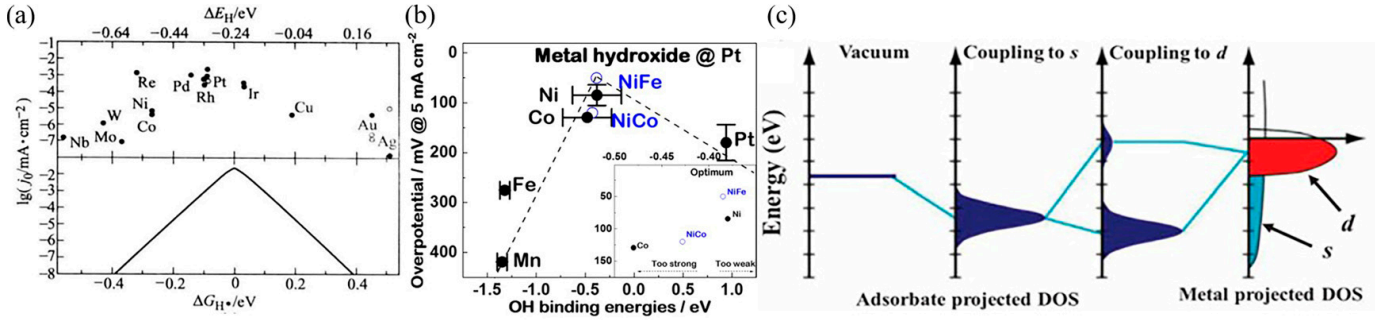

Figure 4. (**a**) Volcano plot between the logarithm of exchange current density of a hydrogen electrode and the Gibbs adsorption free energy of a hydrogen atom based on the DFT calculation [8]. (**b**) "Volcano plot" of Pt–modified with different metal hydroxide clusters (the inset is a partial enlargement corresponding to the top of the volcano) [43]. (**c**) Schematic illustration of the formation of a chemical bond between an adsorbate valence level and the s– and d–states of a transition-metal surface [29]. Copyright 2020, 2021 John Wiley and Sons; 2005 Springer Nature.

It is important to note that OH* may also be an important factor affecting the HER activity, especially in alkaline electrolytes. Xue et al. [43] studied the HER activity of Pt(111), Ni@Pt(111), NiFe@Pt(111) and NiCo@Pt(111) under the same experimental conditions. The relation of the binding energy with OH* was NiCo@Pt(111) > NiFe@Pt(111) > Ni@Pt(111), and the corresponding HER activity was NiFe@Pt(111) > Ni@Pt(111) > Ni-Co@Pt(111) > Pt(111). The Ni clusters on Pt(111) play the role of water decomposition. The introduction of Co increased the adsorption of OH, and the strong adsorption hindered the subsequent reaction steps of Ni-Co clusters. NiFe@Pt is in a better balance between water decomposition and preventing OH* "poisoning". Therefore, the OH* binding energy may be one of the important descriptors of the basic HER (Figure 4b). Too weak OH* binding energy leads to slower water decomposition, while too strong OH* binding energy leads to catalyst "poisoning".

This section may be divided into subheadings. It should provide a concise and precise description of the experimental results, their interpretation, as well as the experimental conclusions that can be drawn.

3.2. D-Band Center Theory

The classical volcanic curve describes the semi-quantitative relationship between the HER rate and ΔG_{H^*} of M-H*, which is essentially closely related to the electronic structure of the metal surface. The DFT calculations also provide greater insight into the electronic structure, particularly how the d-orbital electrons affect the adsorption strength of H* on a given electrode surface.

The d-band model established by Nørskov et al. [29,57] is an approximate description of bonding between adsorbent atoms on a given metal surface. As shown in Figure 4c [29], the valence space orbitals of adsorbent atoms are first coupled with the s-band on the metal surface to form a low-bonding band with energy close to the s-band of the metal, named the reforming band. The reforming band is coupled with the metal d-band, and the energy is further reduced to form a bonding band, with energy lower than the reforming band, and an anti-bonding band with energy higher than the d-orbital, which is called the final bonding band. If the anti-bonding band is less filled with electrons, then the larger the part is above the Fermi level, indicating that the bonding is more stable. If the antibonding band is more filled with electrons, then the smaller the part is above the Fermi level, demonstrating that the bonding is less stable. The stability of the bonding between the adsorbent and the metal surface is influenced by the coupling of the s-band with the valence orbital of the adsorbent and the d-band with the reforming band. Nørskov believed that the energy range and shape of the reforming orbit formed by the valence shell orbit of adsorbates and the s-band of metals in the first step are not very different for all transition

metals. It can be considered that the reforming band formed by all transition metals in the first step is similar. Therefore, the d-band of the second step plays an important role. If the d-band center determines the energy range of the anti-bonding band formed in the second step, then the energy level of the d-band center determines the degree of the anti-bonding band being filled by electrons. It further determines the stability and strength of the adsorption bond, which is the d-band center (ε_d) theory. The interaction between H* orbitals and metal d-orbitals will produce fully filled bonding orbitals with low energy and partially filled anti-bonding orbitals with high energy located above the metal d-band. The strength of the M-H bond depends on the relative occupation of the anti-bonding H 1s-M d. The higher the occupation of anti-bonding orbitals is, the weaker the bonding strength will be. Therefore, the adsorption energy of H* and ΔG_{H^*} of transition metal-based catalysts can be qualitatively predicted and verified by comparing the calculated d-band states density on the metal surface with the Fermi energy levels. Each metal system can adjust its d-band center by alloying and constructing heterogeneous interfaces and optimizing the H* adsorption energy, thus improving the HER performance.

4. Noble Metal-Based Heterogeneous Catalysts

The interaction between surface atom and reactive molecule is crucial to the catalytic performance, which is dependent on the complex atomic arrangement and electronic structure of the surface and interface. However, using single component, it is hard to meet the above requirements. Therefore, interface engineering is used to develop heterogeneous catalysts by means of atom-site mixing of components (alloying strategy) or constructing special structures.

4.1. Alloying Strategy

The most direct way to modify the adsorption behavior is to adjust the outer electronic structure of metal elements. Taking platinum group metals as example, the position of the d-band center reflects the adsorption strength of the platinum group metals. The upshift of the d-band center (i.e., close to the Fermi level) leads to a stronger binding, while the downshift of the d-band center (i.e., far away from the Fermi level) leads to a weaker binding [29]. Therefore, constructing disordered solid solution alloys and ordered intermetallic compounds using exogenous elements have proved to be an effective way to improve the performance of single-component catalysts by optimizing the binding energy [58].

4.1.1. Pt-Base Alloy

At present, commercial Pt/C catalysts are still the most widely used catalysts for the HER. In order to improve the catalytic performance of Pt, a series of Pt-based alloy catalysts have been developed. Pt can be alloyed with different precious metals such as Pd [59], Ru [60], Au [61] and Ag [62], but the high cost is not favorable for large-scale commercialization. To address the cost problem, alloying Pt with non-precious metals such as Fe [63], Co [64], Ni [65], Cu [66] and Ti [67] has also been extensively investigated. The d-band center theory mentioned above shows that the distance of the d-band center relative to the Fermi level is closely related to the adsorption energy. Alloying Pt with transition metals (Co, Fe, Ni and Cu) will cause the d-band center of Pt to downshift and weaken the adsorption energy of oxygen-containing (OH*) on the surface Pt atom. Nørskov and co-authors have calculated a "volcanic" relationship between the d-band center of a bimetallic alloy and the chemisorption of catalyst surface molecules [29]. Wang et al. [68] prepared bimetallic nanoparticles with different compositions and structures, obtained dealloyed samples using pickling, and then prepared bimetallic samples with platinum "skin" using annealing (PtCo sample in Figure 5a). Taking the alkaline HER (in 0.1 M and 1 M KOH, respectively) as an example, the linear relationship between the d-band vacancy and the j_0 was established (Figure 5b,c). The results showed that most of the alloy materials with a thin Pt skin showed strong catalytic activity, while the dealloyed PtCo and PtFe did

not follow the linear relationship and showed higher activity. Selective optimization of the adsorption properties of H* and OH* intermediates is the key to improving the HER activity, and dealloying to enhance the surface atomic activity is undoubtedly a successful strategy.

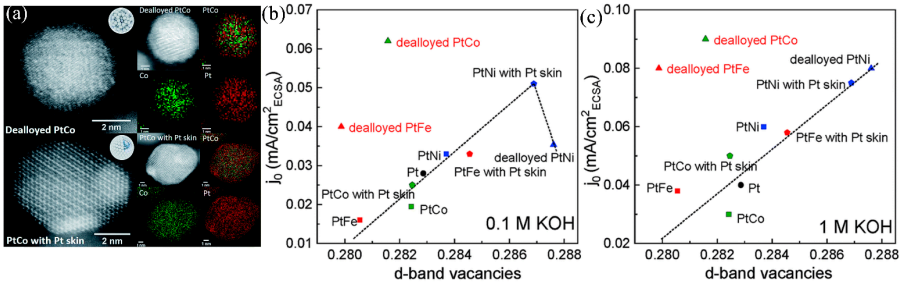

Figure 5. (**a**) HAADF-STEM and EDS mapping images of a dealloyed PtCo sample and PtCo with Pt skin. (**b**,**c**) The experimentally acquired relationship between the d–band vacancies and j_0 for a series of Pt–based materials in (**b**) 0.1 M KOH and (**c**) 1 M KOH solutions [68]. Copyright 2019 Royal Society of Chemistry.

4.1.2. Pd-Based Alloy

Palladium (Pd) is widely found in the Earth's crust and is about one-fifth of the price of Pt. Due to its similar atomic size and lattice mismatch of 0.77%, Pd is a potential alternative material for Pt [69]. In the latest research progress of Pd-based alloys, Qin et al. [70] introduced Ru to improve the HER catalytic activity in an alkaline electrolyte and prepared Pd_3Ru alloy nanoparticles enriched with Ru on the surface. The Ru atoms/clusters on the catalyst surface weakened the hydrogen bonding energy and promoted the adsorption of OH*, thus reducing the reaction barrier of the HER. The overpotential η_{10} of Pd_3Ru alloy in a 1 M KOH solution is 104 mV and 6 mV lower than Pd and Pt, respectively. In addition, non-noble metals can also form alloys with Pd, such as Co, Bi, Ni and Cu [71]. Due to the synergistic effect between the PdNi alloy and carbon materials, the dispersion of the Pd-Ni alloy on carbon materials can improve the HER activity [72]. Alloying with different metals can move the d-band center of Pd downshift (i.e., away from the Fermi level). Alloying can adjust the single element to keep the appropriate hydrogen binding energy of the catalyst and make the intermediate state have the optimal Gibbs free energy, thus improving the HER activity.

4.1.3. Other Pt Group Metal Alloys

In addition to Pt-based alloys and Pd-based alloys, Ir-based alloys have attracted attention in the field of water electrolysis due to their superior intrinsic catalytic activity. At present, Ir alloys with both noble and non-noble metals have been successfully designed, especially with non-noble metals (such as Fe [73], Co [74] and Ni [75]). Alloying not only ensures superior catalytic performance but also has a competitive advantage in cost. Taking IrFe alloy as an example, the overpotential is only 850 mV at the current density of 1000 mA cm^{-2} in 1 M KOH, which is better than commercial Pt/C (η_{1000} = 1.17 V). Due to the difference in electronegativity, the incorporation of Fe significantly modulates the Fermi level of Ir through electron transfer, bringing ΔG_{H^*} closer to 0 and thus enhancing the HER activity [73].

Fine-tuning the composition is also crucial to the catalytic activity of the alloy. Researchers usually choose economical iron elements to form an alloy with precious metals. Shan et al. [76] found that the strength of the HER catalytic activity of RuIr alloy doped with iron elements was Co-RuIr > Ni-RuIr > Fe-RuIr ≈ RuIr. In addition, some research groups have synthesized RhCo alloy nanosheets [77] and RuNi alloy multilayer nanosheets [78]. The RuNi alloy shows excellent HER catalytic activity (η_{10} = 15 mV, Tafel slope: 28 mV dec^{-1}) in 1 M KOH, attributing to the optimization of H_2O dissociation and hydrogen adsorption and desorption during the HER process by RuNi alloying effect [78].

4.1.4. Intermetallic Compound

The alloy can reduce the cost of precious metals and improve the catalytic activity of precious metals, but the disordered structure of a solid solution alloy makes its stability poor. Intermetallic compounds mainly refer to alloy compounds that combine metals and metals or metals and nonmetals (such as H, B, N, S, P, C, Si, etc.) according to a certain atomic stoichiometric ratio to form a crystal lattice different from the original single component. Thermodynamically, solid solution alloys have a higher entropy due to their greatly disordered atomic arrangement, which is more favorable than ordered intermetallic compounds at high temperature. However, under certain compositions and temperatures, the strong d–d interaction between transition metal atoms can provide the required enthalpy change for the alloy system, resulting in a decrease in Gibbs free energy and forming ordered intermetallic junction physical properties. These strong d–d interactions have better stability than disordered solid solution alloys with similar composition and morphology, thus attracting much attention [79].

The synthesis of intermetallic compounds can be divided into two types: annealing after liquid phase synthesis and direct liquid phase synthesis. The difference between the above two methods is the annealing step and the formation mechanism of the ordered structure. The annealing after liquid phase synthesis needs high-temperature treatment under a reduced gas atmosphere. When the annealing temperature is higher than 500 °C, the size and shape of nanostructures are unevenly distributed during the transition from disorder to order, which makes it difficult to accurately control the size and shape of the nanostructures of intermetallic compounds [80]. The direct liquid phase synthesis needs a seed to grow material. During this process, it is hard to control the size of the catalyst. Therefore, developing a synthetic strategy that can accurately control the size and shape of intermetallic compounds is a challenge. Kim et al. [81] used a mesoporous silica template to synthesize a well-defined nanomaterial through nanomaterial space limiting. This method allows precise control of the size and shape of nanostructures by converting disordered alloy Pt_3Co nanowires (D-Pt_3Co-NWs) into ordered intermetallic compound Pt_3Co nanowires (O-Pt_3Co-NWs) without agglomeration (Figure 6a,b). O-Pt_3Co NWs have higher HER activity than O-Pt_3Co NWs and Pt/C catalysts in alkaline conditions (Figure 6c). The enhancement of the O-Pt_3Co NWs HER kinetic is achieved through alloying and atomic ordering regulation of the hydrogen binding energy.

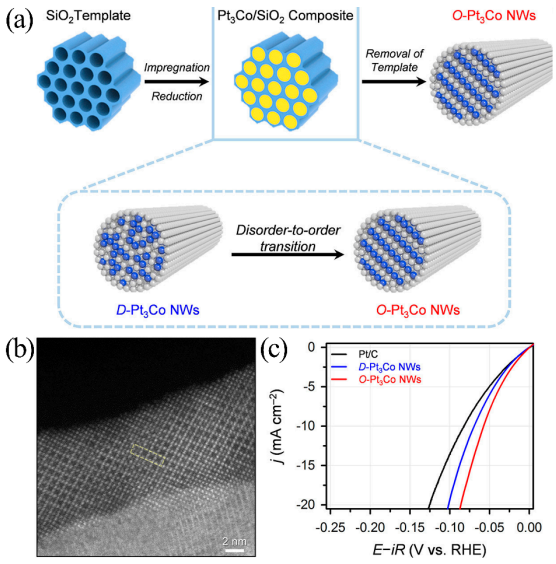

Figure 6. (**a**) Atomic-resolution HAADF-STEM image of O-Pt_3Co NWs; (**b**) HER polarization curves of Pt/C, D–Pt_3Co NWs, and O–Pt_3Co NWs in N_2–saturated 0.1 M KOH electrolyte at a rotation speed of 2500 rpm and a scan rate of 2 mV s^{-1}; (**c**) Corresponding Tafel plots of HER polarization curves [81]. Copyright 2019 American Chemical Society.

Although most research on intermetallic compounds has focused on materials with polymetallic components, some researchers have focused on alloying products formed between metals and non-metals. For example, Ai et al. [82] studied the critical role of electron interaction between metal and boron in surface hydrogenation adsorption and catalytic activity using a combination of theory and experiments. The result shows that the adsorption of hydrogen atoms on the surface of intermetallic compounds is weaker than that on the corresponding pure metal surface. This is due to the strong hybridization between the d-orbital of transition metal and the sp-orbital of boron, which changes the d-band properties. By calculating the ΔG_{H^*} on the surface of boron-containing intermetallic compounds (TMB) of hydrogen atoms, several extremely active hydrogen evolution catalysts (e.g., PdB, RuB) of TMB types are predicted.

In order to better understand and compare these precious metal alloy catalysts, Table 1 lists the essential parameters for evaluating their HER properties.

Table 1. The HER Performance of Various Alloyed Electrocatalysts under Different Reaction Conditions.

Catalyst	Electrolyte	Overpotential (η_{10}/mV)	Tafel Slope (mV·dec^{-1})	Ref.
Pd@PdPt	0.5 M H_2SO_4	39	38	[59]
PtRu	0.5 M H_2SO_4	19.7	27.2	[60]
H-AgPt NCs [a]	0.5 M H_2SO_4	51	40	[62]
PdNi	0.5 M H_2SO_4	55	57	[72]
RhCo ANAs [a]	0.5 M H_2SO_4	12.4	30.7	[77]
RuB	0.5 M H_2SO_4	22	30.7	[82]
Pt_3Ti	0.1 M $HClO_4$	32.7	32.3	[67]
Co-RuIr	0.1 M $HClO_4$	14	31.1	[76]
$Au_{33}Pt_{67}$	0.1 M KOH	171	81	[61]
PtCo	0.1 M KOH	η_{20} = 76.2	76	[64]
O-Pt_3Co-NWs [a]	0.1 M KOH	56.1	30	[81]
$Pt_{24}Cu_{76}$ NFs [a]	0.5 M KOH	18	52	[66]
CoFe–Pt1%	1 M KOH	18	29	[63]
Pd_3Ru	1 M KOH	42	-	[70]
IrFe@NC [a]	1 M KOH	η_{1000} = 850	30	[73]
RuNi	1 M KOH	15	28	[78]

[a] H-AgPt NCs: hollow bimetallic AgPt alloyed nanocrystals, ANAs: alloy nanosheet aggregates, O-Pt_3Co-NWs: ordered intermetallic Pt_3Co nanowires, NFs: nanoframes, NC: N-doped carbon layers.

4.2. Interface Engineering

In addition to the alloying strategy, interface engineering can modify the geometric structure of catalytic materials, reasonably control the atomic arrangement of the surface or interface, optimize the adsorption capacity of reactants, intermediates, and products and effectively improve the efficiency of electrocatalysis. Based on noble metal nanomaterials, this part will be discussed according to the interfacial geometry of the catalyst. Firstly, the coated core–shell nanostructured precious metal particles are introduced, then some typical 2D structure-supported precious metals are introduced, then 1D/3D structure-supported noble metals are introduced, and finally, special atomic interface materials such as single atoms are introduced. A comparison of the HER properties of different interfacial electrocatalysts listed in this paper is summarized in Table 2. The above hybrid nanostructures can be constructed from different materials, such as metal–metal, metal–oxide/hydroxide, metal–sulfide, a metal–metal organic framework, metal–MXene and metal–carbon.

Table 2. The HER Performance of Various Interfacial Electrocatalysts under Different Reaction Conditions.

Catalyst	Electrolyte	Overpotential (η_{10}/mV)	Tafel Slope (mV·dec^{-1})	Ref.
4H/*fcc* Au@PdAg NRBs [a]	0.5 M H_2SO_4	26.2	30	[83]
Pd@Ru NRs [a]	0.5 M H_2SO_4	37	33	[84]
Pt-MoS_2	0.5 M H_2SO_4	-	40	[85]
Pt–MXene–CNTs [a]	0.5 M H_2SO_4	62	66.6	[86]
Ru@C_2N	0.5 M H_2SO_4	22	30	[87]
C_3N_4/Pd	0.5 M H_2SO_4	-	116	[88]
C_3N_4/Pt	0.5 M H_2SO_4	-	71	[88]
Ru@MWCNT [a]	0.5 M H_2SO_4	13	27	[89]
Pt@2D MXene	0.5 M H_2SO_4	80	66.6	[90]
Pt@3D MXene	0.5 M H_2SO_4	13	24.2	[90]
Ru SAs@PN [a]	0.5 M H_2SO_4	24	38	[91]
Pt@MoS_2/NiS_2	0.5 M H_2SO_4	34	40	[92]
Pt/NiS@Al_2O_3	0.5 M H_2SO_4	34	35	[14]
Pd@Ru NPs [a]	0.1 M KOH	41	36	[93]
Pd@Ru NRs [a]	1 M KOH	30	30	[84]
PtRu NCs/BP [a]	1 M KOH	22	19	[94]
Pt–NiFe LDH/CC [a]	1 M KOH	28	39	[95]
Pt/Ni-MOF	1 M KOH	25	42.1	[96]
Ru@C_2N	1 M KOH	17	38	[87]
Ru@MWCNT [a]	1 M KOH	17	27	[89]

[a] NRBs: nanoribbons, NRs: nanorods, CNTs: carbon nanotubes, MWCNT: multiwalled carbon nanotube, PN: phosphorus nitride imide nanotubes, NPs: nanoplates, NCs: nanoclusters, BP: black phosphorus, CC: carbon fiber cloth.

4.2.1. Metal/Metal Core–Shell Nanostructures

Catalysts with core–shell structure are usually composed of core (one composition) and shell (another composition). For the bimetallic compounds of the core–shell structure, their formation is driven by the difference in the surface free enthalpy between the two metals [97,98]. Usually, the component with less enthalpy is going to be the shell. Because the shell has more exposed surface than the core, it needs higher energy. Among them, the precious metal components can exist in the shell to improve the atomic utilization. The noble metal shell can enhance the catalytic activity through electronic coupling with components in the core at the interface or through the strain effect. The common synthesis method of the core–shell structure is to preferentially grow the seed core, and then the noble metal shell grows on the core with chemical reduction or thermal decomposition. At present, numerous efforts have been made in the preparation of core–shell catalysts to achieve the controlled synthesis of composition, morphology, size and shell thickness. In addition to changing the composition, 0D, 1D and 2D core–shell structures have been developed by controlling the morphology.

The 0D core–shell nanostructure mainly consists of nanoparticles and nanopolyhedra. Wang et al. [99] studied Ru-Pt model catalysts with the same ligand effect but different surface geometry. The Ru@Pt core–shell structure with a strain interface has a higher activity than a strain-free alloy (RuPt). The enhancement of HER activity induced by strain in an alkaline electrolyte was larger than that in an acidic electrolyte, ascribing to a more significant interaction between the catalytic intermediates and OH^- caused by compressive strain. Therefore, the basic HER activity can be improved by the strain at the core–shell interface.

The 1D core–shell nanostructure mainly contains nanorods, nanowires and nanoribbons. Zhang and co-works [83] used the Au nanoribbons as templates, on which other noble metals such as Ag, Pd, and Pt with lattice mismatch less than 5% were epitaxially grown. They then obtained a series of core-shell nanoribbons, including Au@Ag, Au@PdAg (Figure 7a–d), Au@PtAg, and Au@PtPdAg. Among them, Au@PdAg nanoribbons show excellent HER electrocatalytic activity (η_{10} = 26.2 mV, Tafel slope = 30 mV dec^{-1}) and durability (nearly no loss of catalytic activity after 10,000 cycles) (Figure 7e–g). Its

excellent catalytic activity is due to its abundant atomic steps, nanodendritic surface, multi-component synergistic effect of the shell and distinct crystal structure. This classic work provides a current strategy for the controlled synthesis of the crystal structure of noble metal nanomaterials. In addition, Luo et al. [84] synthesized mesoporous Pd@Ru core–shell bimetallic nanorods composed of *fcc* Pd and *hcp* Ru. The DFT calculation shows that Ru/Pd (111) interface structure enhanced the alkaline HER activity (η_{10} = 30 mV in 1.0 M KOH).

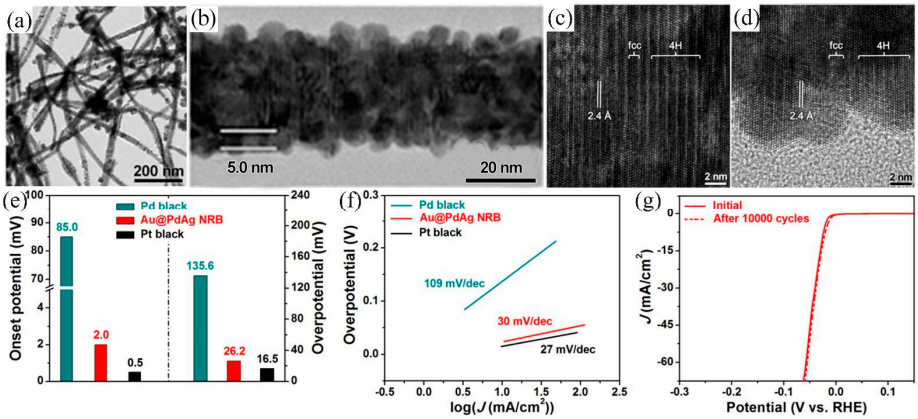

Figure 7. (**a**,**b**) TEM images and (**c**,**d**) HRTEM images of 4H/*fcc* Au@PdAg core–shell nanoribbons. (**e**) Onset potentials and overpotentials (at j = 10 mA cm^{-2}) of Pd black, 4H/*fcc* Au@PdAg NRB, and Pt black. (**f**) Corresponding Tafel plots. (**g**) Durability test of 4H/*fcc* Au@PdAg NRB. All measurements were conducted in a 0.5 M H_2SO_4 aqueous solution [83]. Copyright 2016 American Chemical Society.

The 2D core–shell nanostructure is mainly covered with nanoplates and nanosheets. Ru-based nanoplates have attracted extensive attention in recent years due to their distinct 2D structure and excellent catalytic performance. However, the synthesis of Ru-based nanoplates remains a challenge, especially the controlled synthesis of 2D structures with atomic thickness. Han et al. [93] successfully synthesized core–shell Pd@Ru nanoplates with *fcc* structure with a simple solvothermal method using Pd nanoplates as the substrate. The thickness and crystal structure of the Ru shell can be adjusted by merely changing the amount of Ru precursor. With the increase in the Ru shell thickness, the HER activity of Pd@Ru firstly increased and then decreased. This is because, with the increase in the Ru shell thickness, its crystal structure changed from the *fcc* to the *hcp* phase.

In fact, shell thickness is critical to catalytic activity. The electron coupling and strain effects are different between the shell and core with different thicknesses. A shell with the thickness of a single atomic layer has the highest utilization rate. However, it is not a balanced and stable configuration, and adverse diffusion will occur on the surface atom after long-term operation or at high temperatures. Therefore, adjusting the thickness of the shell accurately requires higher requirements for the structure synthesis and interface structure.

4.2.2. D Structure Hybrid Nanostructures Loaded with Noble Metals

The ultrathin 2D nanomaterials have attracted broad attention since Novoselov et al. [100] mechanically separated graphene from graphite in 2004. In recent years, researchers have developed many ultrathin 2D materials (Figure 8), such as transition metal dichalcogenides, metal-organic frameworks, hexagonal boron nitride, graphite carbon nitride, black phosphorus, MXenes, layered metal oxides and layered double hydroxides [101].

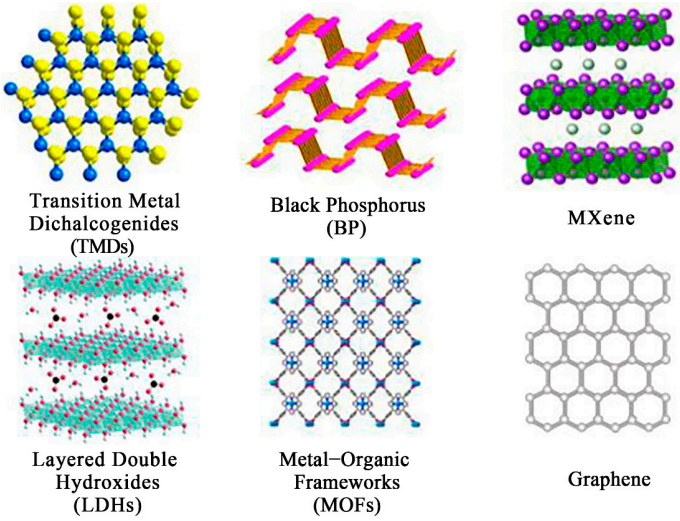

Figure 8. Schematic illustration of different kinds of typical ultrathin 2D nanomaterials, such as TMDs, BP, MXene, LDHs, MOFs and graphene [101,102]. Copyright 2013 Royal Society of Chemistry; 2015 American Chemical Society.

The electronic confinement of ultrathin 2D nanomaterials without interlayer interaction, especially single-layer nanomaterials, gives them better electronic properties than other nanomaterials. In addition, their large lateral size and atomic layer thickness give them an extremely high specific surface area, exposing more surface atoms, which is ideal for expanding their applications in the field of high surface activity [103,104]. Based on the above advantages, researchers choose 2D materials as the substrate for noble metals, which can effectively prevent the agglomeration of noble metals in the catalytic process and improve the catalytic performance by exposing the surface active sites.

- TMDs, Transition Metal Dichalcogenides

TMDs are an essential semiconductor material, whose chemical composition is MX2 (M is the transition metal, X is S, Se or Te), and the 2D structural units (such as S-Mo-S) are combined with each other through van der Waals forces, which has broad application prospects in electrocatalysis. At present, noble metal nanoparticles such as Pt, Pd, Ru and Au have been grown on TMDs (such as MoS_2, $MoSe_2$, WS_2, TiS_2, TaS_2, VS_2 and VSe_2) for the HER [105,106]. For example, Huang et al. [85] synthesized epitaxial-grown Pt-MoS_2 composites using the wet chemical method. Under the same Pt loading, the material showed better HER electrocatalytic activity than the commercial Pt catalyst, mainly due to the strong interaction between MoS_2 nanocrystals and Pt nanoparticles, regulating the electronic state of the Pt nanoparticles ($Pt^0 \rightarrow Pt^{\delta+}$).

- BP, Black Phosphorus

BP has a layered structure, and the layers are combined by van der Waals forces. When BP and other materials (such as Ni_2P [107], Co_2P [108] and MoS_2 [109]) are assembled into heterostructures, the result can promote the performance of electrocatalytic HER. In addition, BP can also be used as a carrier to regulate the electronic structure of noble metals and synergistically promote the HER performance. Li et al. [94] synthesized the hybrid structure of PtRu nanoclusters (NCs) and BP nanosheets (Figure 9a), which showed 10.2 times higher HER activity (η_{10} = 22 mV; Tafel slope = 19 mV dec^{-1}) than that of commercial Pt/C (Figure 9b) in 1 M KOH. The DFT calculations showed that the electronic synergy effect resulting from the strong electron coupling between BP nanosheets and PtRu nanoclusters accelerated the water dissociation, optimized the adsorption strength of H* and enabled the PtRu NCs/BP hybrid material to have high HER activity (Figure 9c,d).

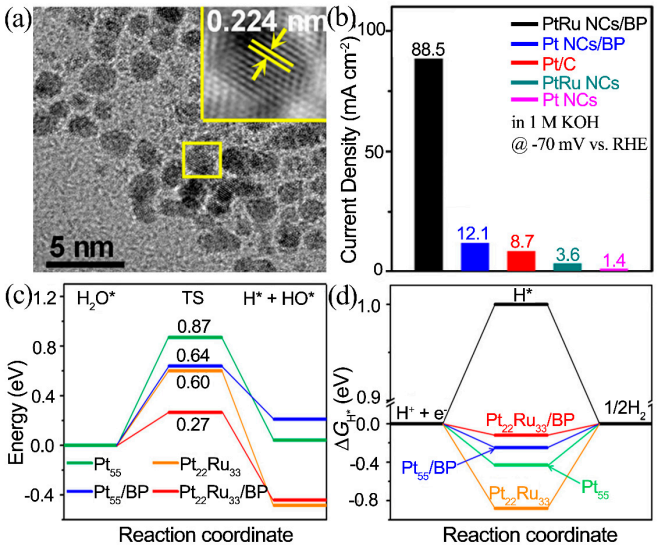

Figure 9. (**a**) HRTEM image of PtRu NCs/BP (Insert: Lattice fringes of the single NC in the yellow frame). (**b**) Current densities of Pt NCs, PtRu NCs, Pt/C, PtRu NCs/BP and Pt NCs/BP at an overpotential of −70 mV. (**c**) Reaction energy diagram of water dissociation on freestanding and BP supported Pt_{55} and $Pt_{22}Ru_{33}$NCs. (**d**) Free energy diagrams for hydrogen evolution at zero potential on the freestanding and BP supported NCs, as well as the bare oxidized BP monolayer [94]. Copyright 2019 American Chemical Society.

- MXene

As typical 2D functional materials, MXene has attracted wide attention in the fields of renewable energy and catalysis [110]. They are a large class of 2D transition metal carbides/nitrides derived from the selectively etched layered MAX phase [111]. MXene can generally be expressed as $M_{n+1}X_nT_x$ (n = 1–3), where M is the transition metal (e.g., Ti, Mo, Nb, Ta or V), X is the C and/or N elements and T represents the surface groups, such as -OH, -O, and -F [112]. MXene has abundant surface chemical properties, high hydrophilicity, mechanical stability, metal conductivity related to high electron density near the Fermi level and other favorable properties [113,114]. For example, Cui et al. [86] mixed a H_2PtCl_6 solution with an MXene solution to form MXene@Pt, and adopted single-walled carbon nanotubes (SWCNTs) as a binder and fluid collector to obtain a layered Pt-MXene-CNT heterostructure. The overpotential is 62 mV at 10 mA cm^{-2} in 0.5 M H_2SO_4, and the Tafel slope is 66.6 mV dec^{-1}. The abundant negatively charged groups on the surface of MXene are conducive to the adsorption of noble metal cations and stabilize the reduced noble metal nanoparticles, effectively preventing their aggregation.

- LDHs, Layered Double Hydroxides

The general formula of LDHs is $[M_{1-x}^{2+}M_x^{3+}(OH)_2]A_x/n^{n-}\cdot mH_2O$, which is composed of a positively charged brucite layered body and exchangeable charge-balanced interlayer anions. A divalent metal ion (e.g., Mg^{2+}, Fe^{2+}, Co^{2+}, Cu^{2+}, Ni^{2+} or Zn^{2+}) is partially coordinated by a hydroxyl octahedron, which can be replaced by a trivalent metal ion (e.g., Al^{3+}, Cr^{3+}, Ga^{3+} or Mn^{3+}) in a brucite layer. One example of the charge-balanced anion is CO_3^{2-}. mH_2O represents the interlayer water molecules [115]. LDHs have attracted extensive attention in the field of electrocatalysis due to their adjustability of metal cations, interlayer anion exchangeability and easy stripping into monolayer nanosheets. However, their poor electrical conductivity restrict their large-scale applications [46]. Researchers have tried to solve this problem by mixing LDH with conductive materials, growing LDH directly on conductive materials (carbon nanotubes, graphene, etc.) or electrode substrates such as nickel foam and carbon fiber cloth [102,116]. For example, Yan et al. [95] grew NiFe LDH in situ on carbon cloth (CC) decorated with ultrafine Pt sub-nanoclusters (average size of 0.59 nm). Highly evenly dispersed Pt can expose more active sites, shorten the

electron transport path and considerably reduce the amount of Pt. In addition, the strong interaction between Pt and 2D NiFe LDH can effectively prevent the aggregation of Pt sub-nanoclusters.

- MOFs, Metal–Organic Frameworks

Metal–organic framework (MOF) materials consisting of central metals, and organic ligands are receiving increasing attention. In particular, 2D MOF nanosheets have become one of the most popular materials in current research, due to their large specific surface area, high proportion of exposed metal atoms, porous structure and adjustable surface functional groups [117]. By introducing additional substrate to construct 2D MOF-based nanocomposites, its intrinsic catalytic activity can be further improved and the feasibility of material application can be expanded [118]. For example, Guo et al. [96] prepared heterogeneous materials (Pt-NC/Ni-MOF) of 2D nickel MOF(Ni-MOF) and Pt nanocrystalline (Pt-NC). The Ni-O-Pt bond formed at the interface regulated the electron distribution and optimized the adsorption of H* and OH* (H* adsorption energy decreased, and OH* adsorption energy increased). The reaction kinetics of the HER was accelerated. The mass activity of the composite was 7.92 mA μg^{-1}_{Pt} at the overpotential of 70 mV, which is one of the best catalysts in alkaline medium reported so far.

- Other 2D materials

In addition to the above materials, there are some other 2D materials such as graphene and its derivatives, including graphene oxide (GO) and reduced graphene oxide (rGO), which have the characteristics of large specific surface area, high carrier mobility and good stability. They are ideal substrates for anchoring functional nanomaterials and are conducive to improving the electrocatalytic activity of materials [119]. For example, Cheng et al. [120] prepared a composite material with defective graphene-supported Pt clusters using the chemical deposition method. The obtained catalyst had favorable HER performance, and its mass activity increased by 11.1 times compared with commercial Pt/C catalyst. In addition, some carbon and nitrogen compounds, such as C_2N [87] and C_3N_4 [88], are also excellent materials for Ru, Pt and Pd catalysts supported.

In summary, 2D materials with rich types, high specific surface area and abundant surface functional groups can not only prevent particles from aggregation but also produce synergistic effect with precious metals when they serve as the supporting substrate of precious metals, thus improving the HER catalytic activity and stability.

4.2.3. 1D/3D Structure Hybrid Nanostructures Loaded with Noble Metals

One-dimensional materials have a high surface area, high roughness factor and high density of active sites. There is a large amount of open space and porosity between adjacent 1D nanostructures, which enables the rapid mass transfer of electrolyte molecules and full contact between chemical substances and the electrode/catalyst surface [121,122]. Recently, Kweon et al. [89] reported that uniform deposition of ruthenium (Ru) nanoparticles on multiwalled carbon nanotubes (Ru@MWCNT) is an efficient HER catalyst. At a current density of 10 mA cm^{-2} in 0.5 M H_2SO_4 and 1 M KOH, Ru@MWCNT exhibits an ultralow overpotential of 13 mV and 17 mV, respectively, exceeding commercial Pt/C (16 mV and 33 mV). The Faraday efficiency (92.28%) was higher than that of the benchmark Pt/C (85.97%) in the actual water electrolysis cell. The DFT calculation shows that the Ru-C bond is the most reasonable active site with the most suitable hydrogen binding energy. Three-dimensional materials can be assembled from one-dimensional or two-dimensional materials. The 3D network has superior mechanical stability and effectively prevents the aggregation and restacking of materials. Moreover, the greatly interconnected structure and porosity of 3D materials make the inner surface of the materials thoroughly utilized and the mass transfer becomes more favorable. Based on these excellent properties of 3D materials, researchers assemble some 1D (such as carbon nanotubes) or 2D (such as graphene, MXene, etc.) materials together to form 3D structures, effectively improving the stability of materials. Kumar et al. [123] prepared noble metals (Pt, Pd, Au and Ag)/3D

graphene (3D-G) nanocomposites and investigated their catalytic activity of the HER. The high conductivity and porous network of 3D graphene sponges provide favorable charge transfer and ions diffusion, further improving the HER catalytic activity and stability. Xiu et al. [90] prepared 3D multistage hollow MXene-loaded Pt nanoparticles (Pt@mh-3D MXene) (Figure 10a,b) and 2D MXene-loaded Pt nanoparticles (Pt@2D MXene) (Figure 10c). The 3D hollow structure can be regarded as the high curvature seal of 2D nanosheets around a well-defined pore space. These MXene are synergistically coupled with ultrafine Pt to form a unique multifunctional catalytic interface design. In particular, Pt@mh-3D MXene not only has the high stability and atomic utilization of Pt but also comprehensively enhances the H* binding capacity, charge transfer capacity and ion/substance transport capacity, promoting HER catalytic activity in the whole pH range. After the optimization, Pt@mh-3D MXene has better HER performance (η_{10} = 13 mV, Tafel slope = 24.2 mV dec^{-1}) than Pt@2D MXene (80 mV, 66.6 mV dec^{-1}) in 0.5 M H_2SO_4. Compared with industrial 20% Pt/C in 1 M KOH, the mass activity and durability are improved by 20 times, while the Pt usage is reduced by 8.3 times (Figure 10d–f).

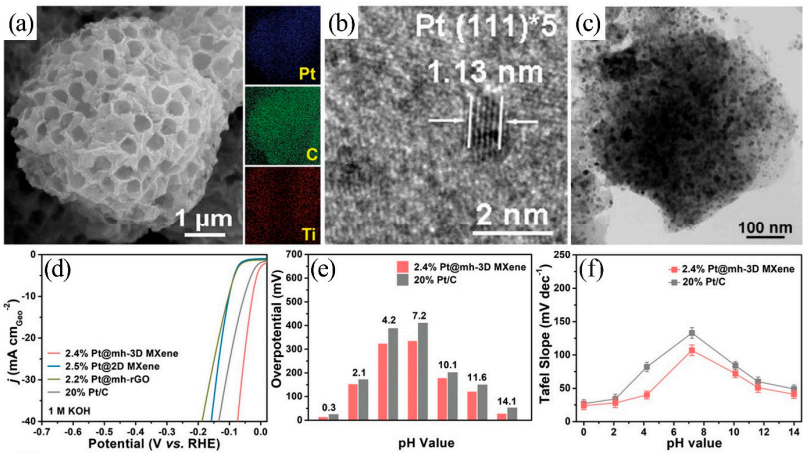

Figure 10. (**a**) SEM image and elemental mapping analysis of Pt@mh–3D MXene. (**b**) HRTEM image of Pt nanocrystallites on mh–3D MXene. (**c**) TEM image of Pt@2D MXene. (**d**) The HER polarization curves of Pt@mh–3D MXene, Pt@2D MXene, Pt@mh-rGO, and Pt/C at a scan rate of 10 mV s^{-1} in 1 M KOH. (**e**,**f**) Comparison between Pt@mh–3D MXene and Pt/C in η_{10} and Tafel slope in the full pH range, respectively [90]. Copyright 2020 John Wiley and Sons.

4.2.4. Single Atom Noble Metal Catalyst

Single-atom doping plays an essential role in catalytic reactions by maximizing atomic efficiency and activating catalytic sites. Atomically dispersed metals are usually anchored to a variety of substrates, including graphene, metal–organic skeleton-derived porous carbon, metal oxides and zeolites, which in most cases can provide pores, vacancy defects or strong interactions [14]. At present, single-atom HER catalysts of the noble metals Pt, Pd, Ru and Ir have been reported, and these single atoms are fixed by coordination with C, N, P, and S atoms on the substrate [124,125]. The reason for improving the activity of a noble metal single-atom catalyst is not only to maximize the utilization of atoms but also to optimize the electronic structure of the noble metal single atom and its heteroatoms by bonding and interacting with the coordination atoms on the substrate, resulting in ΔG_{H^*} being closer to 0 [124]. The coordination structure has a great effect on the catalytic performance. However, it remains a big challenge for researchers to elaborate the design of the coordination number without changing the atomic dispersion [126,127]. Yang et al. [91] prepared the Ru SAs@PN catalyst using amorphous phosphoimide nitrides nanotubes (HPNs) as the substrate of the stabilized Ru single atoms (SAs) (Figure 11a). There is a strong coordination interaction between the lone pair of electrons of N in the HPN substrate and the d-orbitals of Ru, thus anchoring the Ru single atoms. The Ru SAs@PN catalyst shows high HER catalytic activity

(in 0.5 M H_2SO_4, η_{10} = 24 mV) (Figure 11b). The DFT calculation shows that the ΔG_{H^*} of Ru SAs@PN is closer to 0 than that of Ru/C, C and C_3N_4-loaded Ru SAs, which is conducive to hydrogen precipitation (Figure 11c). However, atom-anchored materials still face a great challenge, namely the difficulty of achieving large-scale stable SAs doping at high loads, which tend to aggregate and agglomerate to form particles. Feng et al. [12] reported a new concept of selective single-atom doping with high loads through lattice mismatch of multicomponent heterogeneous nanostructures (e.g., NiS@Al_2O_3 [12], MoS_2/NiS_2 [92], etc.). Due to the special properties of heterogeneous nanostructures, a large number of vacancy defects or voids are generated on the heterogeneous interface so that more atoms can be trapped.

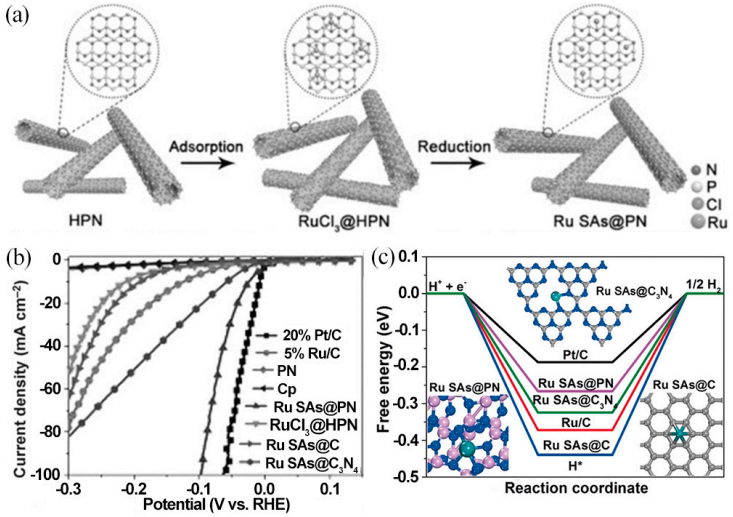

Figure 11. (**a**) Preparation process of Ru SAs@PN. (**b**) Polarization curves at 10 mV s^{-1}. (**c**) The calculated free-energy diagram of the HER at the equilibrium potential for Pt/C, Ru/C, Ru SAs@C, Ru SAs@C_3N_4 and Ru SAs@PN [91]. Copyright 2018 John Wiley and Sons.

5. Conclusions and Prospects

The research progress of noble metal electrocatalysts for hydrogen production using water electrolysis in recent years is reviewed in this paper. For noble metals, great progress has been made in improving the utilization efficiency by reducing particle size to increase surface area, designing a core–shell structure to expose atoms to the shell and binding with conductive substrate to increase the dispersion and stability of the noble metal atoms. We highlighted several methods for designing novel nanostructured catalysts to enhance the active center and optimize the electronic and geometric structure, including the construction of noble metal alloys and core–shell structures with secondary metallic elements to adjust the electronic structure and optimize the thermodynamic hydrogen adsorption/desorption on the catalyst surface. Furthermore, the noble metal and the carrier with a favorable electrical conductivity are combined to form a heterostructure or heterointerface to reduce the load of the noble metal and accelerate the transmission of electrons and ions, so as to reduce the kinetic reaction barrier. In addition, we also mentioned the preparation of working electrodes and the choice of the electrolyte on the performance of aquatic hydrogen electrolysis. Despite the remarkable progress made to date, many challenges remain in this area.

1. Noble metals are expensive, and the preparation process of catalysts is complex. Although various effective noble metal–based catalysts with low metal loading capacity and small size have been developed, the high surface energy leads to the easy aggregation of metal atoms in the catalytic process, resulting in reduced catalytic activity, which makes it difficult to meet the commercial demand. Therefore, it is urgent to

develop a simple synthesis method to prepare small monodisperse catalysts with favorable dispersion and high loading capacity.

2. A thorough understanding of the HER mechanism is of great significance to adjusting catalytic activity and guiding the structural design of prospective catalysts. Although the DFT calculations have been used to predict reaction intermediates and active centers of catalysts and to design efficient HER catalysts, theoretical models are mostly simplifications of actual catalytic conditions. Especially in an alkaline medium, there is no consensus on the HER activity descriptor and action mechanism. At present, most of the catalyst characterization techniques used are situ techniques, which can only provide information before and after the measurement of the catalyst, while ignoring the evolution of the microstructure of the atomic layer on the catalyst surface and the reaction intermediates adsorbed on the catalyst surface during the process. Therefore, there is an urgent need to develop advanced in situ characterization techniques and theoretical simulations to accurately elucidate the reaction mechanism at the molecular level.
3. The development of HER and OER bifunctional catalysts with high activity, selectivity and stability are necessary, which can reduce the costs and simplify setups. The efficiency of hydrogen production depends not only on the cathode catalytic efficiency but also on the anode catalytic efficiency in practical water electrolysis hydrogen production devices and applications. Most HER catalysts (e.g., Pt-based catalysts, chalcogenides, and phosphides) have better catalytic effects in acidic media, while most OER catalysts (e.g., transition metal oxides and (oxy)hydroxides) have better catalytic activity in alkaline media. Under the same experimental conditions, few catalysts can effectively catalyze both the HER and OER. When the two-electrode reactions are paired together in an electrolytic cell with the same electrolyte, the integration is incompatible, thus damping the catalytic performance. Therefore, the development of bifunctional catalysts with excellent HER and OER activities is a future research goal and opportunity.
4. Establishing standardized measurements to compare the HER performance of different electrocatalysts will help to screen and optimize existing catalytic systems and also help to determine and compare the activity of newly developed electrocatalysts.

Author Contributions: Writing—original draft preparation, H.N. and M.Z.; writing—review and editing, H.N., Q.W. and C.H.; visualization, T.L. and Y.Y.; supervision, W.Z. All authors have read and agreed to the published version of the manuscript.

Funding: This research received no external funding.

Acknowledgments: This work was financially supported by the National Natural Science Foundation of China (51972011).

Conflicts of Interest: The authors declare no conflict of interest.

References

1. Niu, H.-J.; Yan, Y.; Jiang, S.; Liu, T.; Sun, T.; Zhou, W.; Guo, L.; Li, J. Interfaces decrease the alkaline hydrogen-evolution kinetics energy barrier on NiCoP/$Ti_3C_2T_x$ MXene. *ACS Nano* **2022**, *16*, 11049–11058. [CrossRef] [PubMed]
2. Li, L.; Wang, P.; Shao, Q.; Huang, X. Metallic nanostructures with low dimensionality for electrochemical water splitting. *Chem. Soc. Rev.* **2020**, *49*, 3072–3106. [CrossRef] [PubMed]
3. Palmer, G.; Roberts, A.; Hoadley, A.; Dargaville, R.; Honnery, D. Life-cycle greenhouse gas emissions and net energy assessment of large-scale hydrogen production via electrolysis and solar PV. *Energy Environ. Sci.* **2021**, *14*, 5113–5131. [CrossRef]
4. Cai, P.; Li, Y.; Wang, G.; Wen, Z. Alkaline–acid Zn–H_2O fuel cell for the simultaneous generation of hydrogen and electricity. *Angew. Chem. Int. Ed.* **2018**, *130*, 3974–3979. [CrossRef]
5. Torella, J.P.; Gagliardi, C.J.; Chen, J.S.; Bediako, D.K.; Colón, B.; Way, J.C.; Silver, P.A.; Nocera, D.G. Efficient solar-to-fuels production from a hybrid microbial–water-splitting catalyst system. *Proc. Natl. Acad. Sci. USA* **2015**, *112*, 2337–2342. [CrossRef]
6. Huang, B.; Wang, P.; Wang, L.; Yang, S.; Wu, D. Recent advances in ocean wave energy harvesting by triboelectric nanogenerator: An overview. *Nanotechnol. Rev.* **2020**, *9*, 716–735. [CrossRef]

7. Feng, Y.; Lin, H.; Ho, S.L.; Yan, J.; Dong, J.; Fang, S.; Huang, Y. Overview of wind power generation in China: Status and development. *Renew. Sustain. Energy Rev.* **2015**, *50*, 847–858. [CrossRef]
8. Shen, S.; Lin, Z.; Song, K.; Wang, Z.; Huang, L.; Yan, L.; Meng, F.; Zhang, Q.; Gu, L.; Zhong, W. Reversed active sites boost the intrinsic activity of graphene-like cobalt selenide for hydrogen evolution. *Angew. Chem. Int. Ed.* **2021**, *133*, 12468–12473. [CrossRef]
9. Li, Y.; Sun, Y.; Qin, Y.; Zhang, W.; Wang, L.; Luo, M.; Yang, H.; Guo, S. Recent advances on water-splitting electrocatalysis mediated by noble-metal-based nanostructured materials. *Adv. Energy Mater.* **2020**, *10*, 1903120. [CrossRef]
10. Sápi, A.; Rajkumar, T.; Kiss, J.; Kukovecz, Á.; Kónya, Z.; Somorjai, G.A. Metallic nanoparticles in heterogeneous catalysis. *Catal. Lett.* **2021**, *151*, 2153–2175. [CrossRef]
11. Zhu, W.; Chen, Z.; Pan, Y.; Dai, R.; Wu, Y.; Zhuang, Z.; Wang, D.; Peng, Q.; Chen, C.; Li, Y. Functionalization of hollow nanomaterials for catalytic applications: Nanoreactor construction. *Adv. Mater.* **2019**, *31*, 1800426. [CrossRef]
12. Feng, Y.; Guan, Y.; Zhang, H.; Huang, Z.; Li, J.; Jiang, Z.; Gu, X.; Wang, Y. Selectively anchoring Pt single atoms at hetero-interfaces of γ-Al_2O_3/NiS to promote the hydrogen evolution reaction. *J. Mater. Chem. A* **2018**, *6*, 11783–11789. [CrossRef]
13. Zhang, L.; Liu, H.; Liu, S.; Norouzi Banis, M.; Song, Z.; Li, J.; Yang, L.; Markiewicz, M.; Zhao, Y.; Li, R. Pt/Pd single-atom alloys as highly active electrochemical catalysts and the origin of enhanced activity. *ACS Catal.* **2019**, *9*, 9350–9358. [CrossRef]
14. Wei, C.; Rao, R.R.; Peng, J.; Huang, B.; Stephens, I.E.; Risch, M.; Xu, Z.J.; Shao-Horn, Y. Recommended practices and benchmark activity for hydrogen and oxygen electrocatalysis in water splitting and fuel cells. *Adv. Mater.* **2019**, *31*, 1806296. [CrossRef]
15. Zheng, J.; Sheng, W.; Zhuang, Z.; Xu, B.; Yan, Y. Universal dependence of hydrogen oxidation and evolution reaction activity of platinum-group metals on pH and hydrogen binding energy. *Sci. Adv.* **2016**, *2*, e1501602. [CrossRef]
16. Xiao, X.; Wang, X.; Jiang, X.; Song, S.; Huang, D.; Yu, L.; Zhang, Y.; Chen, S.; Wang, M.; Shen, Y. In situ growth of Ru nanoparticles on (Fe, Ni)$(OH)_2$ to boost hydrogen evolution activity at high current density in alkaline media. *Small Methods* **2020**, *4*, 1900796. [CrossRef]
17. Yan, Y.; Zhang, R.; Yu, Y.; Sun, Z.; Che, R.; Wei, B.; LaGrow, A.P.; Wang, Z.; Zhou, W. Interfacial optimization of PtNi octahedrons@Ti_3C_2 MXene with enhanced alkaline hydrogen evolution activity and stability. *Appl. Catal. B* **2021**, *291*, 120100. [CrossRef]
18. Zhang, L.; Zhuang, L.; Liu, H.; Zhang, L.; Cai, R.; Chen, N.; Yang, X.; Zhu, Z.; Yang, D.; Yao, X. Beyond Platinum: Defects Abundant CoP_3/Ni_2P Heterostructure for Hydrogen Evolution Electrocatalysis. *Small Sci.* **2021**, *1*, 2000027. [CrossRef]
19. Wang, G.; Wen, Z. Self-supported bimetallic Ni–Co compound electrodes for urea- and neutralization energy-assisted electrolytic hydrogen production. *Nanoscale* **2018**, *10*, 21087–21095. [CrossRef]
20. Zhang, Q.; Xiao, W.; Guo, W.H.; Yang, Y.X.; Lei, J.L.; Luo, H.Q.; Li, N.B. Macroporous array induced multiscale modulation at the surface/interface of $Co(OH)_2$/NiMo self-supporting electrode for effective overall water splitting. *Adv. Funct. Mater.* **2021**, *31*, 2102117. [CrossRef]
21. Ge, J.; Wei, P.; Wu, G.; Liu, Y.; Yuan, T.; Li, Z.; Qu, Y.; Wu, Y.; Li, H.; Zhuang, Z. Ultrathin palladium nanomesh for electrocatalysis. *Angew. Chem. Int. Ed.* **2018**, *130*, 3493–3496. [CrossRef]
22. Mei, P.; Kim, J.; Kumar, N.A.; Pramanik, M.; Kobayashi, N.; Sugahara, Y.; Yamauchi, Y. Phosphorus-based mesoporous materials for energy storage and conversion. *Joule* **2018**, *2*, 2289–2306. [CrossRef]
23. Sun, T.; Zhang, C.; Chen, J.; Yan, Y.; Zakhidov, A.A.; Baughman, R.H.; Xu, L. Three-dimensionally ordered macro-/mesoporous Ni as a highly efficient electrocatalyst for the hydrogen evolution reaction. *J. Mater. Chem. A* **2015**, *3*, 11367–11375. [CrossRef]
24. Lee, J.; Park, J.C.; Bang, J.U.; Song, H. Precise tuning of porosity and surface functionality in Au@SiO_2 nanoreactors for high catalytic efficiency. *Chem. Mater.* **2008**, *20*, 5839–5844. [CrossRef]
25. Shinozaki, K.; Zack, J.W.; Richards, R.M.; Pivovar, B.S.; Kocha, S.S. Oxygen reduction reaction measurements on platinum electrocatalysts utilizing rotating disk electrode technique: I. Impact of impurities, measurement protocols and applied corrections. *J. Electrochem. Soc.* **2015**, *162*, F1144. [CrossRef]
26. Liu, G.; Li, X.; Wang, M.; Wang, M.; Kim, J.Y.; Woo, J.Y.; Wang, X.; Lee, J.K. A study on anode diffusion layer for performance enhancement of a direct methanol fuel cell. *Energy Convers. Manag.* **2016**, *126*, 697–703. [CrossRef]
27. Li, M.; Xia, Z.; Luo, M.; He, L.; Tao, L.; Yang, W.; Yu, Y.; Guo, S. Structural Regulation of Pd-Based Nanoalloys for Advanced Electrocatalysis. *Small Sci.* **2021**, *1*, 2100061. [CrossRef]
28. Li, Y.; Wang, H.; Xie, L.; Liang, Y.; Hong, G.; Dai, H. MoS_2 nanoparticles grown on graphene: An advanced catalyst for the hydrogen evolution reaction. *J. Am. Chem. Soc.* **2011**, *133*, 7296–7299. [CrossRef]
29. Nørskov, J.K.; Abild-Pedersen, F.; Studt, F.; Bligaard, T. Density functional theory in surface chemistry and catalysis. *Proc. Natl. Acad. Sci. USA* **2011**, *108*, 937–943. [CrossRef]
30. Tan, W.; Xie, S.; Le, D.; Diao, W.; Wang, M.; Low, K.-B.; Austin, D.; Hong, S.; Gao, F.; Dong, L. Fine-tuned local coordination environment of Pt single atoms on ceria controls catalytic reactivity. *Nat. Commun.* **2022**, *13*, 7070. [CrossRef]
31. Chen, Z.; Chen, L.; Wen, Z.; Jiang, Q. Understanding electro-catalysis by using density functional theory. *Phys. Chem. Chem. Phys.* **2019**, *21*, 23782–23802. [CrossRef] [PubMed]
32. Li, Y.-R.; Li, M.-X.; Li, S.-N.; Liu, Y.-J.; Chen, J.; Wang, Y. A review of energy and environment electrocatalysis based on high-index faceted nanocrystals. *Rare Met.* **2021**, *40*, 3406–3441. [CrossRef]
33. Kang, J.; Qiu, X.; Hu, Q.; Zhong, J.; Gao, X.; Huang, R.; Wan, C.; Liu, L.-M.; Duan, X.; Guo, L. Valence oscillation and dynamic active sites in monolayer NiCo hydroxides for water oxidation. *Nat. Catal.* **2021**, *4*, 1050–1058. [CrossRef]

34. Zhao, H.; Zhu, Y.; Li, F.; Hao, R.; Wang, S.; Guo, L. A generalized strategy for the synthesis of large-size ultrathin two-dimensional metal oxide nanosheets. *Angew. Chem. Int. Ed.* **2017**, *56*, 8766–8770. [CrossRef] [PubMed]
35. Nai, J.; Tian, Y.; Guan, X.; Guo, L. Pearson's principle inspired generalized strategy for the fabrication of metal hydroxide and oxide nanocages. *J. Am. Chem. Soc.* **2013**, *135*, 16082–16091. [CrossRef]
36. Mao, D.; Wan, J.; Wang, J.; Wang, D. Sequential templating approach: A groundbreaking strategy to create hollow multishelled structures. *Adv. Mater.* **2019**, *31*, 1802874. [CrossRef]
37. Wang, Q.; Liu, K.; Hu, K.; Cai, C.; Li, H.; Li, H.; Herran, M.; Lu, Y.-R.; Chan, T.-S.; Ma, C.; et al. Attenuating metal-substrate conjugation in atomically dispersed nickel catalysts for electroreduction of CO_2 to CO. *Nat. Commun.* **2022**, *13*, 6082. [CrossRef]
38. Dalton, F. Ecs classics: Historical origins of the rotating ring-disk electrode. *Electrochem. Soc. Interface* **2016**, *25*, 50. [CrossRef]
39. Schmidt, T.; Gasteiger, H.; Stäb, G.; Urban, P.; Kolb, D.; Behm, R. Characterization of high-surface-area electrocatalysts using a rotating disk electrode configuration. *J. Electrochem. Soc.* **1998**, *145*, 2354. [CrossRef]
40. Hu, E.; Feng, Y.; Nai, J.; Zhao, D.; Hu, Y.; Lou, X.W.D. Construction of hierarchical Ni–Co–P hollow nanobricks with oriented nanosheets for efficient overall water splitting. *Energy Environ. Sci.* **2018**, *11*, 872–880. [CrossRef]
41. Suntivich, J.; Gasteiger, H.A.; Yabuuchi, N.; Shao-Horn, Y. Electrocatalytic measurement methodology of oxide catalysts using a thin-film rotating disk electrode. *J. Electrochem. Soc.* **2010**, *157*, B1263. [CrossRef]
42. Sheng, W.; Gasteiger, H.A.; Shao-Horn, Y. Hydrogen oxidation and evolution reaction kinetics on platinum: Acid vs alkaline electrolytes. *J. Electrochem. Soc.* **2010**, *157*, B1529. [CrossRef]
43. Xue, S.; Haid, R.W.; Kluge, R.M.; Ding, X.; Garlyyev, B.; Fichtner, J.; Watzele, S.; Hou, S.; Bandarenka, A.S. Enhancing the hydrogen evolution reaction activity of platinum electrodes in alkaline media using nickel–iron clusters. *Angew. Chem. Int. Ed.* **2020**, *59*, 10934–10938. [CrossRef]
44. Ye, R.; del Angel-Vicente, P.; Liu, Y.; Arellano-Jimenez, M.J.; Peng, Z.; Wang, T.; Li, Y.; Yakobson, B.I.; Wei, S.H.; Yacaman, M.J. High-performance hydrogen evolution from $MoS_{2(1-x)}P_x$ solid solution. *Adv. Mater.* **2016**, *28*, 1427–1432. [CrossRef] [PubMed]
45. Sun, H.; Yan, Z.; Liu, F.; Xu, W.; Cheng, F.; Chen, J. Self-supported transition-metal-based electrocatalysts for hydrogen and oxygen evolution. *Adv. Mater.* **2020**, *32*, 1806326. [CrossRef]
46. Shen, X.; Li, H.; Zhang, Y.; Ma, T.; Li, Q.; Jiao, Q.; Zhao, Y.; Li, H.; Feng, C. Construction dual-regulated $NiCo_2S_4$@Mo-doped CoFe-LDH for oxygen evolution reaction at large current density. *Appl. Catal. B* **2022**, *319*, 121917. [CrossRef]
47. Zhu, X.; Tang, C.; Wang, H.-F.; Li, B.-Q.; Zhang, Q.; Li, C.; Yang, C.; Wei, F. Monolithic-structured ternary hydroxides as freestanding bifunctional electrocatalysts for overall water splitting. *J. Mater. Chem. A* **2016**, *4*, 7245–7250. [CrossRef]
48. Durst, J.; Siebel, A.; Simon, C.; Hasché, F.; Herranz, J.; Gasteiger, H. New insights into the electrochemical hydrogen oxidation and evolution reaction mechanism. *Energy Environ. Sci.* **2014**, *7*, 2255–2260. [CrossRef]
49. Garlyyev, B.; Xue, S.; Pohl, M.D.; Reinisch, D.; Bandarenka, A.S. Oxygen electroreduction at high-index Pt electrodes in alkaline electrolytes: A decisive role of the alkali metal cations. *ACS Omega* **2018**, *3*, 15325–15331. [CrossRef]
50. Xue, S.; Garlyyev, B.; Watzele, S.; Liang, Y.; Fichtner, J.; Pohl, M.D.; Bandarenka, A.S. Influence of alkali metal cations on the hydrogen evolution reaction activity of Pt, Ir, Au, and Ag electrodes in alkaline electrolytes. *ChemElectroChem* **2018**, *5*, 2326–2329. [CrossRef]
51. Garlyyev, B.; Fichtner, J.; Piqué, O.; Schneider, O.; Bandarenka, A.S.; Calle-Vallejo, F. Revealing the nature of active sites in electrocatalysis. *Chem. Sci.* **2019**, *10*, 8060–8075. [CrossRef]
52. Li, A.; Sun, Y.; Yao, T.; Han, H. Earth-abundant transition-metal-based electrocatalysts for water electrolysis to produce renewable hydrogen. *Chem.-A Eur. J.* **2018**, *24*, 18334–18355. [CrossRef]
53. Parsons, R. The rate of electrolytic hydrogen evolution and the heat of adsorption of hydrogen. *Trans. Faraday Soc.* **1958**, *54*, 1053–1063. [CrossRef]
54. Subbaraman, R.; Tripkovic, D.; Chang, K.-C.; Strmcnik, D.; Paulikas, A.P.; Hirunsit, P.; Chan, M.; Greeley, J.; Stamenkovic, V.; Markovic, N.M. Trends in activity for the water electrolyser reactions on 3d M (Ni, Co, Fe, Mn) hydr (oxy) oxide catalysts. *Nat. Mater.* **2012**, *11*, 550–557. [CrossRef]
55. Cao, X.; Tan, Y.; Zheng, H.; Hu, J.; Chen, X.; Chen, Z. Effect of cobalt phosphide (CoP) vacancies on its hydrogen evolution activity via water splitting: A theoretical study. *Phys. Chem. Chem. Phys.* **2022**, *24*, 4644–4652. [CrossRef]
56. Zheng, Y.; Jiao, Y.; Zhu, Y.; Li, L.H.; Han, Y.; Chen, Y.; Jaroniec, M.; Qiao, S.-Z. High electrocatalytic hydrogen evolution activity of an anomalous ruthenium catalyst. *J. Am. Chem. Soc.* **2016**, *138*, 16174–16181. [CrossRef] [PubMed]
57. Medford, A.J.; Vojvodic, A.; Hummelshøj, J.S.; Voss, J.; Abild-Pedersen, F.; Studt, F.; Bligaard, T.; Nilsson, A.; Nørskov, J.K. From the Sabatier principle to a predictive theory of transition-metal heterogeneous catalysis. *J. Catal.* **2015**, *328*, 36–42. [CrossRef]
58. Fan, L.; Ji, Y.; Wang, G.; Chen, J.; Chen, K.; Liu, X.; Wen, Z. High entropy alloy electrocatalytic electrode toward alkaline glycerol valorization coupling with acidic hydrogen production. *J. Am. Chem. Soc.* **2022**, *144*, 7224–7235. [CrossRef]
59. Liu, Y.; Liu, S.; Che, Z.; Zhao, S.; Sheng, X.; Han, M.; Bao, J. Concave octahedral Pd@PdPt electrocatalysts integrating core–shell, alloy and concave structures for high-efficiency oxygen reduction and hydrogen evolution reactions. *J. Mater. Chem. A* **2016**, *4*, 16690–16697. [CrossRef]
60. Li, K.; Li, Y.; Wang, Y.; Ge, J.; Liu, C.; Xing, W. Enhanced electrocatalytic performance for the hydrogen evolution reaction through surface enrichment of platinum nanoclusters alloying with ruthenium in situ embedded in carbon. *Energy Environ. Sci.* **2018**, *11*, 1232–1239. [CrossRef]

61. Wu, W.; Tang, Z.; Wang, K.; Liu, Z.; Li, L.; Chen, S. Peptide templated AuPt alloyed nanoparticles as highly efficient bi-functional electrocatalysts for both oxygen reduction reaction and hydrogen evolution reaction. *Electrochim. Acta* **2018**, *260*, 168–176. [CrossRef]
62. Shao, F.-Q.; Zhu, X.-Y.; Wang, A.-J.; Fang, K.-M.; Yuan, J.; Feng, J.-J. One-pot synthesis of hollow AgPt alloyed nanocrystals with enhanced electrocatalytic activity for hydrogen evolution and oxygen reduction reactions. *J. Colloid Interface Sci.* **2017**, *505*, 307–314. [CrossRef] [PubMed]
63. Zhang, Q.; Kuang, Y.; Li, Y.; Jiang, M.; Cai, Z.; Pang, Y.; Chang, Z.; Sun, X. Synthesis and performance optimization of ultrathin two-dimensional CoFePt alloy materials via in situ topotactic conversion for the hydrogen evolution reaction. *J. Mater. Chem. A* **2019**, *7*, 9517–9522. [CrossRef]
64. Chen, Q.; Cao, Z.; Du, G.; Kuang, Q.; Huang, J.; Xie, Z.; Zheng, L. Excavated octahedral Pt-Co alloy nanocrystals built with ultrathin nanosheets as superior multifunctional electrocatalysts for energy conversion applications. *Nano Energy* **2017**, *39*, 582–589. [CrossRef]
65. Cao, Z.; Chen, Q.; Zhang, J.; Li, H.; Jiang, Y.; Shen, S.; Fu, G.; Lu, B.-A.; Xie, Z.; Zheng, L. Platinum-nickel alloy excavated nano-multipods with hexagonal close-packed structure and superior activity towards hydrogen evolution reaction. *Nat. Commun.* **2017**, *8*, 15131. [CrossRef]
66. Huang, X.-Y.; You, L.-X.; Zhang, X.-F.; Feng, J.-J.; Zhang, L.; Wang, A.-J. L-proline assisted solvothermal preparation of Cu-rich rhombic dodecahedral PtCu nanoframes as advanced electrocatalysts for oxygen reduction and hydrogen evolution reactions. *Electrochim. Acta* **2019**, *299*, 89–97. [CrossRef]
67. Li, Z.; Qi, Z.; Wang, S.; Ma, T.; Zhou, L.; Wu, Z.; Luan, X.; Lin, F.-Y.; Chen, M.; Miller, J.T. In situ formed Pt_3Ti nanoparticles on a two-dimensional transition metal carbide (MXene) used as efficient catalysts for hydrogen evolution reactions. *Nano Lett.* **2019**, *19*, 5102–5108. [CrossRef]
68. Wang, X.; He, Q.; Song, L.; Jaroniec, M.; Zheng, Y.; Qiao, S.-Z. Breaking the volcano-plot limits for Pt-based electrocatalysts by selective tuning adsorption of multiple intermediates. *J. Mater. Chem. A* **2019**, *7*, 13635–13640. [CrossRef]
69. Zhang, L.; Roling, L.T.; Wang, X.; Vara, M.; Chi, M.; Liu, J.; Choi, S.-I.; Park, J.; Herron, J.A.; Xie, Z. Platinum-based nanocages with subnanometer-thick walls and well-defined, controllable facets. *Science* **2015**, *349*, 412–416. [CrossRef]
70. Qin, X.; Zhang, L.; Xu, G.-L.; Zhu, S.; Wang, Q.; Gu, M.; Zhang, X.; Sun, C.; Balbuena, P.B.; Amine, K. The role of Ru in improving the activity of Pd toward hydrogen evolution and oxidation reactions in alkaline solutions. *ACS Catal.* **2019**, *9*, 9614–9621. [CrossRef]
71. Zhang, L.; Chang, Q.; Chen, H.; Shao, M. Recent advances in palladium-based electrocatalysts for fuel cell reactions and hydrogen evolution reaction. *Nano Energy* **2016**, *29*, 198–219. [CrossRef]
72. Chen, J.; Chen, J.; Yu, D.; Zhang, M.; Zhu, H.; Du, M. Carbon nanofiber-supported PdNi alloy nanoparticles as highly efficient bifunctional catalysts for hydrogen and oxygen evolution reactions. *Electrochim. Acta* **2017**, *246*, 17–26. [CrossRef]
73. Jiang, P.; Huang, H.; Diao, J.; Gong, S.; Chen, S.; Lu, J.; Wang, C.; Sun, Z.; Xia, G.; Yang, K. Improving electrocatalytic activity of iridium for hydrogen evolution at high current densities above 1000 mA cm^{-2}. *Appl. Catal. B* **2019**, *258*, 117965. [CrossRef]
74. Jiang, P.; Chen, J.; Wang, C.; Yang, K.; Gong, S.; Liu, S.; Lin, Z.; Li, M.; Xia, G.; Yang, Y. Tuning the activity of carbon for electrocatalytic hydrogen evolution via an iridium-cobalt alloy core encapsulated in nitrogen-doped carbon cages. *Adv. Mater.* **2018**, *30*, 1705324. [CrossRef]
75. Gong, S.; Wang, C.; Jiang, P.; Yang, K.; Lu, J.; Huang, M.; Chen, S.; Wang, J.; Chen, Q. O species-decorated graphene shell encapsulating iridium–nickel alloy as an efficient electrocatalyst towards hydrogen evolution reaction. *J. Mater. Chem. A* **2019**, *7*, 15079–15088. [CrossRef]
76. Shan, J.; Ling, T.; Davey, K.; Zheng, Y.; Qiao, S.Z. Transition-metal-doped RuIr bifunctional nanocrystals for overall water splitting in acidic environments. *Adv. Mater.* **2019**, *31*, 1900510. [CrossRef]
77. Zhao, Y.; Bai, J.; Wu, X.-R.; Chen, P.; Jin, P.-J.; Yao, H.-C.; Chen, Y. Atomically ultrathin RhCo alloy nanosheet aggregates for efficient water electrolysis in broad pH range. *J. Mater. Chem. A* **2019**, *7*, 16437–16446. [CrossRef]
78. Liu, G.; Zhou, W.; Chen, B.; Zhang, Q.; Cui, X.; Li, B.; Lai, Z.; Chen, Y.; Zhang, Z.; Gu, L. Synthesis of RuNi alloy nanostructures composed of multilayered nanosheets for highly efficient electrocatalytic hydrogen evolution. *Nano Energy* **2019**, *66*, 104173. [CrossRef]
79. Li, J.; Sun, S. Intermetallic nanoparticles: Synthetic control and their enhanced electrocatalysis. *Acc. Chem. Res.* **2019**, *52*, 2015–2025. [CrossRef]
80. Xiao, W.; Lei, W.; Gong, M.; Xin, H.L.; Wang, D. Recent advances of structurally ordered intermetallic nanoparticles for electrocatalysis. *ACS Catal.* **2018**, *8*, 3237–3256. [CrossRef]
81. Kim, H.Y.; Kim, J.M.; Ha, Y.; Woo, J.; Byun, A.; Shin, T.J.; Park, K.H.; Jeong, H.Y.; Kim, H.; Kim, J.Y.; et al. Activity origin and multifunctionality of Pt-based intermetallic nanostructures for efficient electrocatalysis. *ACS Catal.* **2019**, *9*, 11242–11254. [CrossRef]
82. Ai, X.; Zou, X.; Chen, H.; Su, Y.; Feng, X.; Li, Q.; Liu, Y.; Zhang, Y.; Zou, X. Transition-metal–boron intermetallics with strong interatomic d–sp orbital hybridization for high-performance electrocatalysis. *Angew. Chem. Int. Ed.* **2020**, *59*, 3961–3965. [CrossRef] [PubMed]
83. Fan, Z.; Luo, Z.; Huang, X.; Li, B.; Chen, Y.; Wang, J.; Hu, Y.; Zhang, H. Synthesis of 4H/fcc noble multimetallic nanoribbons for electrocatalytic hydrogen evolution reaction. *J. Am. Chem. Soc.* **2016**, *138*, 1414–1419. [CrossRef]

84. Luo, Y.; Luo, X.; Wu, G.; Li, Z.; Wang, G.; Jiang, B.; Hu, Y.; Chao, T.; Ju, H.; Zhu, J.; et al. Mesoporous Pd@Ru core–shell nanorods for hydrogen evolution reaction in alkaline solution. *ACS Appl. Mater. Interfaces* **2018**, *10*, 34147–34152. [CrossRef]
85. Huang, X.; Zeng, Z.; Bao, S.; Wang, M.; Qi, X.; Fan, Z.; Zhang, H. Solution-phase epitaxial growth of noble metal nanostructures on dispersible single-layer molybdenum disulfide nanosheets. *Nat. Commun.* **2013**, *4*, 1444. [CrossRef]
86. Cui, C.; Cheng, R.; Zhang, H.; Zhang, C.; Ma, Y.; Shi, C.; Fan, B.; Wang, H.; Wang, X. Ultrastable MXene@Pt/SWCNTs' nanocatalysts for hydrogen evolution reaction. *Adv. Funct. Mater.* **2020**, *30*, 2000693. [CrossRef]
87. Mahmood, J.; Li, F.; Jung, S.-M.; Okyay, M.S.; Ahmad, I.; Kim, S.-J.; Park, N.; Jeong, H.Y.; Baek, J.-B. An efficient and pH-universal ruthenium-based catalyst for the hydrogen evolution reaction. *Nat. Nanotechnol.* **2017**, *12*, 441–446. [CrossRef]
88. Nazir, R.; Fageria, P.; Basu, M.; Gangopadhyay, S.; Pande, S. Decoration of Pd and Pt nanoparticles on a carbon nitride (C_3N_4) surface for nitro-compounds reduction and hydrogen evolution reaction. *New J. Chem.* **2017**, *41*, 9658–9667. [CrossRef]
89. Kweon, D.H.; Okyay, M.S.; Kim, S.-J.; Jeon, J.-P.; Noh, H.-J.; Park, N.; Mahmood, J.; Baek, J.-B. Ruthenium anchored on carbon nanotube electrocatalyst for hydrogen production with enhanced Faradaic efficiency. *Nat. Commun.* **2020**, *11*, 1278. [CrossRef]
90. Xiu, L.; Pei, W.; Zhou, S.; Wang, Z.; Yang, P.; Zhao, J.; Qiu, J. Multilevel hollow MXene tailored Low-Pt catalyst for efficient hydrogen evolution in full-pH range and seawater. *Adv. Funct. Mater.* **2020**, *30*, 1910028. [CrossRef]
91. Yang, J.; Chen, B.; Liu, X.; Liu, W.; Li, Z.; Dong, J.; Chen, W.; Yan, W.; Yao, T.; Duan, X.; et al. Efficient and robust hydrogen evolution: Phosphorus nitride imide nanotubes as supports for anchoring single ruthenium sites. *Angew. Chem. Int. Ed.* **2018**, *57*, 9495–9500. [CrossRef] [PubMed]
92. Guan, Y.; Feng, Y.; Wan, J.; Yang, X.; Fang, L.; Gu, X.; Liu, R.; Huang, Z.; Li, J.; Luo, J.; et al. Ganoderma-like MoS_2/NiS_2 with single platinum atoms doping as an efficient and stable hydrogen evolution reaction catalyst. *Small* **2018**, *14*, 1800697. [CrossRef] [PubMed]
93. Han, Y.; Yan, Y.; Wu, Z.; Jiang, Y.; Li, X.; Xu, Q.; Yang, X.; Zhang, H.; Yang, D. Facile synthesis of Pd@Ru nanoplates with controlled thickness as efficient catalysts for hydrogen evolution reaction. *CrystEngComm* **2018**, *20*, 4230–4236. [CrossRef]
94. Li, Y.; Pei, W.; He, J.; Liu, K.; Qi, W.; Gao, X.; Zhou, S.; Xie, H.; Yin, K.; Gao, Y. Hybrids of PtRu nanoclusters and black phosphorus nanosheets for highly efficient alkaline hydrogen evolution reaction. *ACS Catal.* **2019**, *9*, 10870–10875. [CrossRef]
95. Yan, Q.; Yan, P.; Wei, T.; Wang, G.; Cheng, K.; Ye, K.; Zhu, K.; Yan, J.; Cao, D.; Li, Y. A highly efficient and durable water splitting system: Platinum sub-nanocluster functionalized nickel–iron layered double hydroxide as the cathode and hierarchical nickel–iron selenide as the anode. *J. Mater. Chem. A* **2019**, *7*, 2831–2837. [CrossRef]
96. Guo, C.; Jiao, Y.; Zheng, Y.; Luo, J.; Davey, K.; Qiao, S.-Z. Intermediate modulation on noble metal hybridized to 2D metal-organic framework for accelerated water electrocatalysis. *Chem* **2019**, *5*, 2429–2441. [CrossRef]
97. Tymoczko, A.; Kamp, M.; Rehbock, C.; Kienle, L.; Cattaruzza, E.; Barcikowski, S.; Amendola, V. One-step synthesis of Fe–Au core–shell magnetic-plasmonic nanoparticles driven by interface energy minimization. *Nanoscale Horiz.* **2019**, *4*, 1326–1332. [CrossRef]
98. Kukovecz, Á.; Kordás, K.; Kiss, J.; Kónya, Z. Atomic scale characterization and surface chemistry of metal modified titanate nanotubes and nanowires. *Surf. Sci. Rep.* **2016**, *71*, 473–546. [CrossRef]
99. Wang, X.; Zhu, Y.; Vasileff, A.; Jiao, Y.; Chen, S.; Song, L.; Zheng, B.; Zheng, Y.; Qiao, S.-Z. Strain effect in bimetallic electrocatalysts in the hydrogen evolution reaction. *ACS Energy Lett.* **2018**, *3*, 1198–1204. [CrossRef]
100. Novoselov, K.S.; Geim, A.K.; Morozov, S.V.; Jiang, D.-e.; Zhang, Y.; Dubonos, S.V.; Grigorieva, I.V.; Firsov, A.A. Electric field effect in atomically thin carbon films. *Science* **2004**, *306*, 666–669. [CrossRef]
101. Zhang, H. Ultrathin Two-Dimensional Nanomaterials. *ACS Nano* **2015**, *9*, 9451–9469. [CrossRef]
102. Li, X.; Du, D.; Zhang, Y.; Xing, W.; Xue, Q.; Yan, Z. Layered double hydroxides toward high-performance supercapacitors. *J. Mater. Chem. A* **2017**, *5*, 15460–15485. [CrossRef]
103. Geim, A.K.; Novoselov, K.S. The rise of graphene. *Nat. Mater.* **2007**, *6*, 183–191. [CrossRef]
104. Li, H.; Zhang, M.; Yi, L.; Liu, Y.; Chen, K.; Shao, P.; Wen, Z. Ultrafine Ru nanoparticles confined in 3D nitrogen-doped porous carbon nanosheet networks for alkali-acid Zn-H_2 hybrid battery. *Appl. Catal. B* **2021**, *280*, 119412. [CrossRef]
105. Lin, L.; Sherrell, P.; Liu, Y.; Lei, W.; Zhang, S.; Zhang, H.; Wallace, G.G.; Chen, J. Engineered 2D transition metal dichalcogenides—A vision of viable hydrogen evolution reaction catalysis. *Adv. Energy Mater.* **2020**, *10*, 1903870. [CrossRef]
106. Yi, L.; Ji, Y.; Shao, P.; Chen, J.; Li, J.; Li, H.; Chen, K.; Peng, X.; Wen, Z. Scalable synthesis of tungsten disulfide nanosheets for alkali-acid electrocatalytic sulfion recycling and H_2 generation. *Angew. Chem. Int. Ed.* **2021**, *60*, 21550–21557. [CrossRef]
107. Lin, Y.; Pan, Y.; Zhang, J. In-situ grown of Ni_2P nanoparticles on 2D black phosphorus as a novel hybrid catalyst for hydrogen evolution. *Int. J. Hydrogen. Energy* **2017**, *42*, 7951–7956. [CrossRef]
108. Wang, J.; Liu, D.; Huang, H.; Yang, N.; Yu, B.; Wen, M.; Wang, X.; Chu, P.K.; Yu, X.-F. In-plane black phosphorus/dicobalt phosphide heterostructure for efficient electrocatalysis. *Angew. Chem. Int. Ed.* **2018**, *57*, 2600–2604. [CrossRef]
109. He, R.; Hua, J.; Zhang, A.; Wang, C.; Peng, J.; Chen, W.; Zeng, J. Molybdenum disulfide–black phosphorus hybrid nanosheets as a superior catalyst for electrochemical hydrogen evolution. *Nano Lett.* **2017**, *17*, 4311–4316. [CrossRef]
110. Anasori, B.; Lukatskaya, M.R.; Gogotsi, Y. 2D metal carbides and nitrides (MXenes) for energy storage. *Nat. Rev. Mater.* **2017**, *2*, 16098. [CrossRef]
111. Xiong, D.; Li, X.; Bai, Z.; Lu, S. Recent advances in layered $Ti_3C_2T_x$ MXene for electrochemical energy storage. *Small* **2018**, *14*, 1703419. [CrossRef] [PubMed]

112. Lukatskaya, M.R.; Mashtalir, O.; Ren, C.E.; Dall'Agnese, Y.; Rozier, P.; Taberna, P.L.; Naguib, M.; Simon, P.; Barsoum, M.W.; Gogotsi, Y. Cation intercalation and high volumetric capacitance of two-dimensional titanium carbide. *Science* **2013**, *341*, 1502–1505. [CrossRef] [PubMed]
113. Pang, S.-Y.; Wong, Y.-T.; Yuan, S.; Liu, Y.; Tsang, M.-K.; Yang, Z.; Huang, H.; Wong, W.-T.; Hao, J. Universal strategy for HF-free facile and rapid synthesis of two-dimensional MXenes as multifunctional energy materials. *J. Am. Chem. Soc.* **2019**, *141*, 9610–9616. [CrossRef] [PubMed]
114. Ran, J.; Gao, G.; Li, F.-T.; Ma, T.-Y.; Du, A.; Qiao, S.-Z. Ti_3C_2 MXene co-catalyst on metal sulfide photo-absorbers for enhanced visible-light photocatalytic hydrogen production. *Nat. Commun.* **2017**, *8*, 13907. [CrossRef]
115. Long, X.; Wang, Z.; Xiao, S.; An, Y.; Yang, S. Transition metal based layered double hydroxides tailored for energy conversion and storage. *Mater. Today* **2016**, *19*, 213–226. [CrossRef]
116. Liu, Y.; Teng, X.; Mi, Y.; Chen, Z. A new architecture design of Ni–Co LDH-based pseudocapacitors. *J. Mater. Chem. A* **2017**, *5*, 24407–24415. [CrossRef]
117. Zhao, S.; Wang, Y.; Dong, J.; He, C.-T.; Yin, H.; An, P.; Zhao, K.; Zhang, X.; Gao, C.; Zhang, L.; et al. Ultrathin metal–organic framework nanosheets for electrocatalytic oxygen evolution. *Nat. Energy* **2016**, *1*, 16184. [CrossRef]
118. Jin, S.; Son, H.-J.; Farha, O.K.; Wiederrecht, G.P.; Hupp, J.T. Energy transfer from quantum dots to metal–organic frameworks for enhanced light harvesting. *J. Am. Chem. Soc.* **2013**, *135*, 955–958. [CrossRef]
119. Stankovich, S.; Dikin, D.A.; Dommett, G.H.B.; Kohlhaas, K.M.; Zimney, E.J.; Stach, E.A.; Piner, R.D.; Nguyen, S.T.; Ruoff, R.S. Graphene-based composite materials. *Nature* **2006**, *442*, 282–286. [CrossRef]
120. Cheng, Q.; Hu, C.; Wang, G.; Zou, Z.; Yang, H.; Dai, L. Carbon-defect-driven electroless deposition of Pt atomic clusters for highly efficient hydrogen evolution. *J. Am. Chem. Soc.* **2020**, *142*, 5594–5601. [CrossRef]
121. Li, J.; Zheng, G. One-dimensional earth-abundant nanomaterials for water-splitting electrocatalysts. *Adv. Sci.* **2017**, *4*, 1600380. [CrossRef]
122. Zhang, M.; Chen, J.; Li, H.; Cai, P.; Li, Y.; Wen, Z. Ru-RuO_2/CNT hybrids as high-activity pH-universal electrocatalysts for water splitting within 0.73 V in an asymmetric-electrolyte electrolyzer. *Nano Energy* **2019**, *61*, 576–583. [CrossRef]
123. Kumar, S.; Sahoo, P.K.; Satpati, A.K. Insight into the catalytic performance of HER catalysis of noble metal/3D-G nanocomposites. *Electrochim. Acta* **2020**, *333*, 135467. [CrossRef]
124. Wang, Y.; Su, H.; He, Y.; Li, L.; Zhu, S.; Shen, H.; Xie, P.; Fu, X.; Zhou, G.; Feng, C.; et al. Advanced electrocatalysts with single-metal-atom active sites. *Chem. Rev.* **2020**, *120*, 12217–12314. [CrossRef]
125. Wei, Z.-X.; Zhu, Y.-T.; Liu, J.-Y.; Zhang, Z.-C.; Hu, W.-P.; Xu, H.; Feng, Y.-Z.; Ma, J.-M. Recent advance in single-atom catalysis. *Rare Met.* **2021**, *40*, 767–789. [CrossRef]
126. Li, S.; Xu, Y.; Wang, H.; Teng, B.; Liu, Q.; Li, Q.; Xu, L.; Liu, X.; Lu, J. Tuning the CO_2 hydrogenation selectivity of rhodium single-atom catalysts on zirconium dioxide with alkali ions. *Angew. Chem. Int. Ed.* **2023**, e202218167. [CrossRef]
127. Zhang, H.; Zhang, X.; Sun, Q.; He, Q.; Ji, H.; He, X. Boosting hydrogenation properties of Pt single-atom catalysts via tailoring the electronic structures by coordination number regulation. *Chem. Eng. J.* **2023**, *455*, 140808. [CrossRef]

Disclaimer/Publisher's Note: The statements, opinions and data contained in all publications are solely those of the individual author(s) and contributor(s) and not of MDPI and/or the editor(s). MDPI and/or the editor(s) disclaim responsibility for any injury to people or property resulting from any ideas, methods, instructions or products referred to in the content.